COMMUN. MATH. SCI.
Vol. 15, No. 4, pp. 985–1019

HIGH-ORDER ACCURATE METHODS BASED ON DIFFERENCE POTENTIALS FOR 2D PARABOLIC INTERFACE MODELS*

JASON ALBRIGHT†, YEKATERINA EPSHTEYN‡, AND QING XIA§

Abstract. Highly-accurate numerical methods that can efficiently handle problems with interfaces and/or problems in domains with complex geometry are essential for the resolution of a wide range of temporal and spatial scales in many partial differential equations based models from Biology, Materials Science and Physics. In this paper we continue our work started in 1D, and we develop high-order accurate methods based on the Difference Potentials for 2D parabolic interface/composite domain problems. Extensive numerical experiments are provided to illustrate high-order accuracy and efficiency of the developed schemes.

Keywords. parabolic problems; interface models; discontinuous solutions; difference potentials; finite differences; high-order accuracy in the solution and in the gradient of the solution; non-matching grids; parallel algorithms

AMS subject classifications. 65M06; 65M22; 65M55; 65M70; 65M12; 35K20.

1. Introduction

Designing numerical methods with high-order accuracy for problems with interfaces (for example, models for composite materials or fluids, etc.), as well as models in domains with complex geometry is crucial for modeling of problems from Biology, Materials Science and Physics. Furthermore, interface problems result in non-smooth solutions (or even discontinuous solutions) at the interfaces, and therefore standard numerical methods (finite-difference, finite-element methods, etc.) in any dimension will very often fail to produce accurate approximations of the solutions to the interface problems, and thus special numerical algorithms have to be developed for the approximation of such problems.

There is extensive literature that addresses problems in domains with irregular geometries and interface problems. For example, among finite-difference/finite-volume based methods for such problems are the Immersed Boundary Method (IB) ([33, 34], etc.), the Immersed Interface Method (IIM) ([1, 20, 23–25], etc.), the Ghost Fluid Method (GFM) ([15,27,28], etc.), the Matched Interface and Boundary Method (MIB) ([46,48], etc.), the method based on the Integral Equations approach, ([30], etc.) and among the most recent methods are Cartesian Grid Embedded Boundary Method ([9]), Multigrid Method for Elliptic Problems with Discontinuous Coefficients on an Arbitrary Interface ([8]), the Virtual Node Method in [18] and the Voronoi Interface Method in [17]. Among the finite-element methods for interface problems are ([5, 7, 43, 45, 47], etc.). These methods are robust interface methods that have been applied to solve many problems in science and engineering. For a detailed review of the subject the reader can consult, for example, [25]. However, in spite of great advances in the numerical methods for interface problems and problems in domains with complex geometry, it is

*Received: December 15, 2015; accepted (in revised form): October 28, 2016. Communicated by John Lowengrub.

†Department of Mathematics, The University of Utah, Salt Lake City, UT, 84112, USA (albright@math.utah.edu).

‡Department of Mathematics, The University of Utah, Salt Lake City, UT, 84112, USA (epshteyn@math.utah.edu).

§Department of Mathematics, The University of Utah, Salt Lake City, UT, 84112, USA (xia@math.utah.edu).

still a challenge (especially for time-dependent problems) to design high-order accurate and efficient methods for such problems.

We develop in this work numerical algorithms based on the Difference Potentials Method (DPM). DPM was originally proposed by V.S. Ryaben'kii in 1969 in his Doctor of Science Habilitation Thesis, see [37,38,41]. DPM on its own, or in combination with other numerical methods, is an efficient technique for the numerical solution, as well as for the discrete modeling of interior and exterior boundary value problems in domains with arbitrary geometry. The main idea behind DPM is to reduce uniquely solvable and well-posed boundary value problems to pseudo-differential boundary equations with projections. Methods based on Difference Potentials introduce computationally simple auxiliary domains. After that, the original domains are embedded into auxiliary domains (and the auxiliary domains are discretized using regular structured grids). Next, DPM defines a Difference Potentials operator and constructs discrete pseudo-differential *Boundary Equations with Projections* to obtain the value of the solution at the points near the continuous boundary of the original domain (at the points of the discrete grid boundary which straddles the continuous boundary from the inside and outside of the domain). Using the reconstructed values of the solution at the discrete grid boundary, the approximation to the solution in the domain is obtained through the discrete generalized Green's formula (see about DPM, for example in, [14,16,38,41] and about recent developments on DPM in [2,3,6,10,12,13,19,29,31,32,39,40,42,44], etc.).

In this paper, we start by extending the work on high-order accurate Difference Potentials methods started in 1D in [3] to 2D linear parabolic interface models (with fixed smooth curvilinear interfaces) and we construct both second-order (DPM2) and fourth-order (DPM4) accurate methods (in time and space) for such problems. *At this point we are not aware of any other fourth-order method for such 2D parabolic interface problems. Moreover, numerical experiments in Section 6 indicate that the developed methods preserve high-order accuracy on the interface problems not only in the solution, but also in the discrete gradient of the solution.*

The main complexity of the high-order methods based on Difference Potentials developed in this work reduces to several solutions of simple auxiliary problems on structured Cartesian grids. The proposed numerical methods are not restricted by the type of the boundary or interface conditions (as long as the continuous problems are well-posed), and are also computationally efficient since any change of the boundary/interface conditions affects only a particular component of the overall algorithm, and does not affect most of the numerical algorithm. Furthermore, the construction of the *Boundary Equations with Projections on the discrete grid boundaries* makes it possible to reconstruct the solution near the interface (from both sides) with high-order accuracy. Finally, the developed methods based on Difference Potentials approach handle non-matching interfaces/(and/or) grids with ease and are well-suited for the development of parallel algorithms.

The paper is organized as follows. In Section 2, we introduce the formulation of the problem. Next, to illustrate the unified approach behind the construction of DPM with different orders of accuracy, we construct methods based on Difference Potentials with second- and with fourth-order accuracy in space and time in Section 3.1 and in Appendix Section 7 for single domain 2D parabolic models. In Section 4, we extend the developed methods to 2D parabolic interface/composite domain model problems. For the reader's convenience, we give a brief summary of the main steps of the presented numerical algorithms in Section 5. Finally, we illustrate the performance of the proposed Difference Potentials Methods, DPM2 and DPM4 in several challenging numerical experiments in

Section 6. Some concluding remarks are given in Section 7.

2. Parabolic interface and composite domain models

In this work we are concerned with the numerical solution of the parabolic interface/composite domain problems on Ω defined inside some bounded auxiliary domain $\Omega^0 \subset \mathbb{R}^2$:

$$\frac{\partial u_{\Omega_1}}{\partial t} - L^1 u_{\Omega_1} = f_{\Omega_1}(x,y,t), \ (x,y) \in \Omega_1 \text{ and } t \in (0,T] \tag{2.1}$$

$$\frac{\partial u_{\Omega_2}}{\partial t} - L^2 u_{\Omega_2} = f_{\Omega_2}(x,y,t), \ (x,y) \in \Omega_2 \text{ and } t \in (0,T] \tag{2.2}$$

subject to the appropriate interface/matching conditions on Γ:

$$\alpha_1 u_{\Omega_1} - \beta_1 u_{\Omega_2} = \mu_1(x,y,t), \ (x,y) \in \Gamma \text{ and } t \in (0,T] \tag{2.3}$$

$$\alpha_2 \frac{\partial u_{\Omega_1}}{\partial n} - \beta_2 \frac{\partial u_{\Omega_2}}{\partial n} = \mu_2(x,y,t), \ (x,y) \in \Gamma \text{ and } t \in (0,T], \tag{2.4}$$

boundary condition on the exterior boundary $\partial\Omega_1$:

$$l(u_{\Omega_1}) = \psi_1(x,y,t), \ (x,y) \in \partial\Omega_1 \text{ and } t \in (0,T], \tag{2.5}$$

and initial conditions:

$$u_{\Omega_1}(x,y,0) = u^0_{\Omega_1}(x,y), \ (x,y) \in \Omega_1 \tag{2.6}$$

$$u_{\Omega_2}(x,y,0) = u^0_{\Omega_2}(x,y), \ (x,y) \in \Omega_2 \tag{2.7}$$

Here, for brevity of notation, we use $u_{\Omega_1} := u_{\Omega_1}(x,y,t)$ to denote the solution to (2.1)-(2.7) in domain Ω_1 and $u_{\Omega_2} := u_{\Omega_2}(x,y,t)$ to denote the solution to (2.1)-(2.7) in domain Ω_2. Operator l in (2.5) is the boundary operator that defines boundary conditions on the exterior boundary $\partial\Omega_1$ (for example, Dirichlet or Neumann, etc.). We consider, here, the composite domain $\Omega = \overline{\Omega_1} \cup \overline{\Omega_2}$ separated by an interface curve Γ, which is a closed smooth curve (we assume in this work that the interface curve Γ is at least in C^2) and $\Omega \subseteq \Omega^0$, see Figure 2.1. We assume in this work that L^s , $s \in \{1,2\}$ are second-order linear elliptic differential operators of the form

$$L^s u_{\Omega_s} \equiv \nabla \cdot (\lambda_s \nabla u_{\Omega_s}), \quad s \in \{1,2\}. \tag{2.8}$$

Here, $\lambda_s > 0$ are positive piecewise-constant coefficients defined in larger auxiliary subdomains $\Omega^0_s \supset \Omega_s$. The sources $f_{\Omega_s}(x,y,t)$ are sufficiently smooth functions defined in each subdomain Ω_s, the functions $\mu_s(x,y,t)$ are sufficiently smooth functions defined on Γ and the function $\psi_1(x,y,t)$ is a sufficiently smooth function defined on $\partial\Omega_1$. For the sake of simplicity, we assume that $\alpha_1, \alpha_2, \beta_1, \beta_2$ are constant coefficients in this work. We assume that the continuous problem (2.1)–(2.7) is well-posed (see for example, [21] and [22] for some existence, uniqueness and regularity results). Furthermore, we consider operators on the left-hand side of (2.1)–(2.2) that are well-defined on some larger auxiliary domain Ω^0_s: we assume that for sufficiently smooth functions $f_{\Omega^0_s}(x,y,t)$ on Ω^0_s, the Equations (2.1)–(2.2) defined on domains Ω^0_s have unique solutions $u_{\Omega^0_s}$ on Ω^0_s that satisfy the given initial, interface and boundary conditions on $\partial\Omega^0_s$. Here and below, the index $s \in \{1,2\}$ is introduced to distinguish between the subdomains.

Remark 2.1.

(1) The introduction of the auxiliary domains Ω^0_s will play an important role in the construction of the proposed methods based on Difference Potentials in Sections 3.1-4 (note that, on Figure 2.1, the auxiliary domains $\Omega^0_1 = \Omega^0_2 \equiv \Omega^0$).

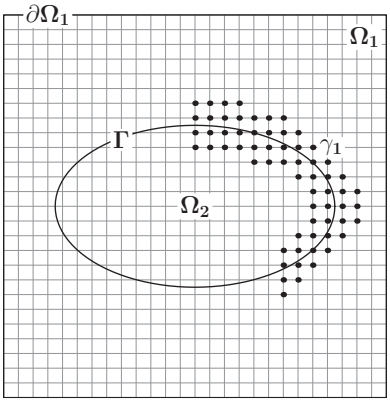

FIG. 2.1. *An example of a bounded composite domain Ω: sub-domains Ω_1 and Ω_2 are separated by an interface defined by a smooth closed curve Γ, and an example of the points in the discrete grid boundary γ_1 for the 9-point stencil of the fourth-order method (the discrete grid boundary straddles the interior boundary Γ of the exterior domain Ω_1). Auxiliary domains $\Omega_1^0 = \Omega_2^0 \equiv \Omega^0$ can be selected here to coincide with the domain Ω (square), see Sections 3.1-4 for the details of the construction.*

(2) Note, that methods developed in this paper are well-suited for variable coefficient problems and models in heterogenous media [11, 12, 41], as well as for nonlinear parabolic models, and these will be a part of the future study [4].

3. Single domain

To simplify the construction of the high-order methods for parabolic interface problems, we first develop high-order methods for parabolic models in a single domain. In Section 4 we generalize this approach to parabolic interface and composite domain problems (2.1)–(2.7).

Consider a linear second-order parabolic equation defined in a domain $\Omega \subset \mathbb{R}^2$:

$$\frac{\partial u}{\partial t} - Lu = f(x,y,t), \ (x,y) \in \Omega \text{ and } t \in (0,T] \tag{3.1}$$

subject to the appropriate boundary conditions:

$$l(u) = \psi(x,y,t), \ (x,y) \in \Gamma \text{ and } t \in (0,T], \tag{3.2}$$

and initial conditions:

$$u(x,y,0) = u^0(x,y), \ (x,y) \in \Omega. \tag{3.3}$$

where $\Omega \subset \Omega^0$ and $\Gamma := \partial\Omega$, see Figure 3.1. Here, again, we use $u := u(x,y,t)$ to denote the solution to (3.1)-(3.3) in the domain Ω and the operator l in (3.2) is the boundary operator that defines boundary conditions on the exterior boundary $\partial\Omega$.

Similar to the interface problem (2.1)–(2.7) we assume that L in (3.1) is the second-order linear elliptic differential operator of the form

$$Lu \equiv \nabla \cdot (\lambda \nabla u), \tag{3.4}$$

where $\lambda > 0$ is a positive constant on $\Omega \subset \Omega^0$. The source function $f(x,y,t)$ is a sufficiently smooth function defined in domain Ω and the function $\psi(x,y,t)$ is a sufficiently

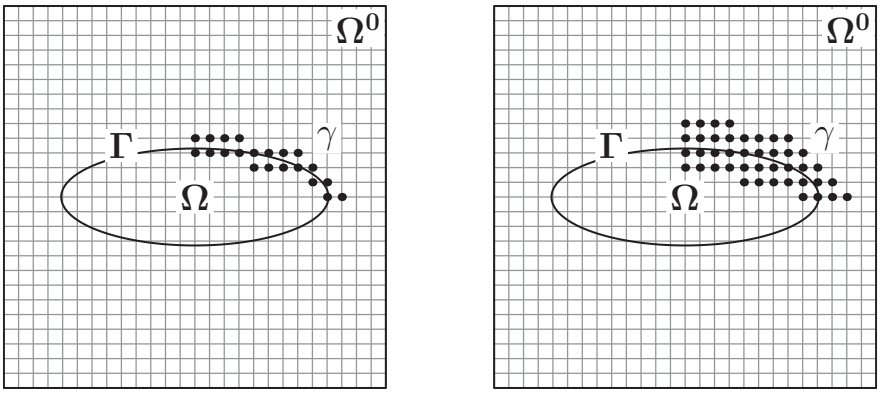

FIG. 3.1. *An example of an auxiliary domain Ω^0, the original domain $\Omega \subset \Omega^0$, a smooth closed boundary curve Γ (we assume in this work that the curve Γ is at least in C^2), and an example of the points in the discrete grid boundary set γ for the 5-point stencil of the second-order method (left figure), and an example of the points in the discrete grid boundary set γ for the 9-point stencil of the fourth-order method (right figure).*

smooth function defined on Γ. We assume that the continuous problem (3.1)–(3.3) is well-posed. Moreover, we consider here the operator on the left-hand side of the Equation (3.1) that is well-defined on some larger auxiliary domain: we assume that for any sufficiently smooth function $f(x,y,t)$ on Ω^0, the Equation (3.1) defined on a larger domain Ω^0 has a unique solution u on Ω^0 satisfying the given initial conditions and boundary conditions on $\partial\Omega^0$.

3.1. High-order accurate methods based on difference potentials for parabolic problems. The current work is an extension of the work started in 1D settings in [3] to the 2D parabolic models. For the time being we restrict our attention here to problems with piecewise-constant coefficients. However, the construction of the methods given below allows for the direct extension to parabolic problems in heterogeneous media, which will be a part of our near future research. In this work, the choices of the underlying second-order or the fourth-order in space and time approximation, (3.9)–(3.10) combined with (3.13), or (3.9)–(3.10) combined with (3.15) were employed with the goal of efficient illustration and implementation of the ideas, as well as for the ease of the future extension to models in heterogeneous media. Note, that the approach presented here based on Difference Potentials can be similarly used with any other suitable underlying high-order discretization of the given continuous model.

Similar to [3], we will illustrate our ideas below by constructing the second and the fourth-order schemes together, and will only comment on the differences between them.

Introduction of the Auxiliary Domain: Place the original domain Ω in the computationally simple auxiliary domain $\Omega^0 \subset \mathbb{R}^2$ that we will choose to be a square. Next, introduce a Cartesian mesh for Ω^0, with points $x_j = j\Delta x, y_k = k\Delta y, (k,j = 0,1,...)$. Let us assume for simplicity that $h := \Delta x = \Delta y$. Define a finite-difference stencil $N^\kappa_{j,k} := N^5_{j,k}$ or $N^\kappa_{j,k} := N^9_{j,k}$ with its center placed at (x_j, y_k), to be a 5-point central finite-difference stencil of the second-order method, or a 9-point central finite-difference stencil of the fourth-order method, respectively, see Figure 3.2:

$$N^\kappa_{j,k} := \{(x_j,y_k),(x_{j\pm1},y_k),(x_j,y_{k\pm1})\}, \quad \kappa = 5, \text{ or} \tag{3.5}$$

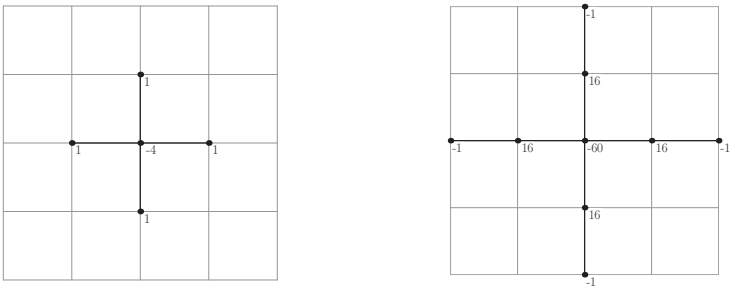

FIG. 3.2. *Example (a sketch) of the* 5*-point stencil for the second-order scheme (3.5) (left figure) and example (a sketch) of the* 9*-point stencil for the fourth-order scheme (3.6) (right figure), [2].*

$$N_{j,k}^{\kappa} := \{(x_j, y_k), (x_{j\pm1}, y_k), (x_j, y_{k\pm1}), (x_{j\pm2}, y_k), (x_j, y_{k\pm2})\}, \quad \kappa = 9. \tag{3.6}$$

Next, introduce the point sets M^0 (the set of all mesh nodes (x_j, y_k) that belong to the interior of the auxiliary domain Ω^0), $M^+ := M^0 \cap \Omega$ (the set of all the mesh nodes (x_j, y_k) that belong to the interior of the original domain Ω), and $M^- := M^0 \backslash M^+$ (the set of all the mesh nodes (x_j, y_k) that are inside of the auxiliary domain Ω^0 but belong to the exterior of the original domain Ω). Define $N^+ := \{\bigcup_{j,k} N_{j,k}^{\kappa} | (x_j, y_k) \in M^+\}$ (the set of all points covered by the stencil $N_{j,k}^{\kappa}$ when the center point (x_j, y_k) of the stencil goes through all the points of the set $M^+ \subset \Omega$). Similarly define $N^- := \{\bigcup_{j,k} N_{j,k}^{\kappa} | (x_j, y_k) \in M^-\}$ (the set of all points covered by the stencil $N_{j,k}^{\kappa}$ when center point (x_j, y_k) of the stencil goes through all the points of the set M^-).

Now, we can introduce $\gamma := N^+ \cap N^-$. The set γ is called the *discrete grid boundary*. The mesh nodes from set γ straddle the boundary $\Gamma \equiv \partial\Omega$. Finally, define $N^0 := \{\bigcup_{j,k} N_{j,k}^{\kappa} | (x_j, y_k) \in M^0\}$.

REMARK 3.1. From here on, κ either takes the value 5 (if the 5-point stencil is used to construct the second-order method), or 9 (if the 9-point stencil is used to construct the fourth-order method).

The sets N^0, M^0, N^+, N^-, M^+, M^-, γ will be used to develop high-order methods in 2D based on the Difference Potentials idea.

Construction of the System of the Discrete Equations: We first discretize Equation (3.1) in time, which yields a time-discrete reformulation of the parabolic Equation (3.1) of the form:

Given numerical solutions u^n, $n \le i$ at previous time levels, find u^{i+1} such that

$$L_{\Delta t}[u^{i+1}] = F^{i+1} \tag{3.7}$$

Here, the operator $L_{\Delta t}[u^{i+1}]$ denotes the linear elliptic operator applied to $u^{i+1} \approx u(\cdot, t^{i+1})$ and F^{i+1} is the right-hand side obtained after time-discretization of (3.1) (see Appendix Section 7 for details). Note, in this paper, we consider the second-order trapezoidal scheme or the second-order backward difference scheme (BDF2) as the time discretization for the construction of the second-order accurate in space Difference Potentials Method (DPM2). The fourth-order backward difference discretization in time (BDF4) is considered for the construction of the fourth-order accurate in space Difference Potentials Method (DPM4). Therefore, the linear operator $L_{\Delta t}[u^{i+1}]$ in (3.7) in

this work takes the general form:

$$L_{\Delta t}[u^{i+1}] \equiv \Big(\Delta - \sigma^2 \mathbb{I}\Big) u^{i+1}, \tag{3.8}$$

with $\mathbb{I}$ being the identity operator and constant coefficient σ^2 defined for each time discretization as follows. For the trapezoidal scheme in time the coefficient is $\sigma^2 := \frac{2}{\lambda \Delta t}$, for BDF2 it is $\sigma^2 := \frac{3}{2\lambda \Delta t}$ and for BDF4 the coefficient is $\sigma^2 := \frac{25}{12\lambda \Delta t}$.

Next, the fully discrete version of (3.1) is: find $u_{j,k}^{i+1}$, $(x_j, y_k) \in N^+$, $t^{i+1} \in (0, T]$ such that

$$L_{\Delta t,h}[u_{j,k}^{i+1}] = F_{j,k}^{i+1}, \ (x_j, y_k) \in M^+. \tag{3.9}$$

The fully discrete system of the Equations (3.9) is obtained here by discretizing (3.7) with either the second-order centered finite difference in space (3.13) or with the fourth-order "direction by direction" approximation in space (3.15). Hence, similar to a time-discrete linear operator $L_{\Delta t}[u^{i+1}]$ in (3.7)–(3.8), the fully discrete linear operator $L_{\Delta t,h}[u_{j,k}^{i+1}]$ in (3.9) in this work takes the general form:

$$L_{\Delta t,h}[u_{j,k}^{i+1}] \equiv \Big(\Delta_h - \sigma^2 \mathbb{I}\Big) u_{j,k}^{i+1}, \tag{3.10}$$

with coefficient σ^2 defined as above for each time discretization. The fully discrete right-hand side in (3.9) takes a form as given below for each time and space discretization:

(1) Second-order discretization in space with trapezoidal time discretization:

$$F_{j,k}^{i+1} := -\frac{1}{\lambda}\Big(f(x_j, y_k, t^{i+1}) + f(x_j, y_k, t^i)\Big) - \Big(\Delta_h + \sigma^2 \mathbb{I}\Big) u_{j,k}^i. \tag{3.11}$$

(2) Second-order discretization in space with BDF2 time discretization:

$$F_{j,k}^{i+1} := -\frac{1}{\lambda} f(x_j, y_k, t^{i+1}) - \frac{\sigma^2}{3}(4u_{j,k}^i - u_{j,k}^{i-1}). \tag{3.12}$$

The operator Δ_h in the above discretization schemes (3.10) and (3.11), and in (3.10) and (3.12) is approximated with second-order accuracy in space using the centered 5-point stencil (3.5):

$$\Delta_h u_{j,k}^{i+1} := \frac{1}{h^2}\left(u_{j-1,k}^{i+1} + u_{j+1,k}^{i+1} + u_{j,k-1}^{i+1} + u_{j,k+1}^{i+1} - 4u_{j,k}^{i+1}\right), \qquad \kappa = 5. \tag{3.13}$$

(3) Fourth-order discretization in space with BDF4 time discretization:

$$F_{j,k}^{i+1} := -\frac{1}{\lambda} f(x_j, y_k, t^{i+1}) - \frac{\sigma^2}{25}(48u_{j,k}^i - 36u_{j,k}^{i-1} + 16u_{j,k}^{i-2} - 3u_{j,k}^{i-3}). \tag{3.14}$$

The Laplace operator in the above discretization scheme (3.10) and (3.14) is approximated with fourth-order accuracy using the 9-point direction-by-direction stencil (3.15):

$$\begin{aligned}\Delta_h u_{j,k}^{i+1} := \frac{1}{12h^2}\big(&-u_{j-2,k}^{i+1} + 16u_{j-1,k}^{i+1} + 16u_{j+1,k}^{i+1} - u_{j+2,k}^{i+1} - u_{j,k-2}^{i+1} \\ &+ 16u_{j,k-1}^{i+1} + 16u_{j,k+1}^{i+1} - u_{j,k+2}^{i+1} - 60u_{j,k}^{i+1}\big), \qquad \kappa = 9.\end{aligned} \tag{3.15}$$

REMARK 3.2. The choice of the time discretization made here has several appealing numerical advantages in terms of stability for diffusion-type operators of the form in (3.1). However, the framework based on Difference Potentials developed in this work is not restricted to these particular choices and the main ideas can be extended directly to other suitable time discretizations.

In general, the linear system of the discrete Equations (3.9) will have multiple solutions. Once we close the discrete system (3.9) with the appropriate discrete boundary conditions, the method will result in an approximation of the continuous model (3.1)–(3.3) in domain Ω. To do so very accurately and efficiently, we will construct numerical algorithms based on the idea of the Difference Potentials.

General Discrete Auxiliary Problem: Some of the important steps of the DPM are the introduction of the auxiliary problem, which we will denote as (AP), as well as definitions of the particular solution and Difference Potentials. Let us recall these definitions below (see also [2,3,41], etc.).

DEFINITION 3.1. *The problem of solving (3.16)–(3.17) is referred to as the discrete auxiliary problem (AP): at each time level t^{i+1} for the given grid function q^{i+1} defined on M^0, find the solution v^{i+1} defined on N^0 of the discrete (AP) such that it satisfies the following system of equations:*

$$L_{\Delta t,h}[v_{j,k}^{i+1}] = q_{j,k}^{i+1}, \quad (x_j,y_k) \in M^0, \tag{3.16}$$

$$v_{j,k}^{i+1} = 0, \quad (x_j,y_k) \in N^0 \backslash M^0. \tag{3.17}$$

Here, $L_{\Delta t,h}$ is the same linear discrete operator as in (3.9), but now it is defined on the larger auxiliary domain $\overline{\Omega^0}$. It is applied in (3.16) to the function v^{i+1} defined on N^0. We remark that under the above assumptions on the continuous model, the (AP) (3.16)–(3.17) is well-defined for any right-hand side function q^{i+1} on M^0: it has a unique solution v^{i+1} defined on N^0. In this work we supplemented the discrete (AP) (3.16) by the zero boundary conditions (3.17). In general, the boundary conditions for (AP) are selected to guarantee that the discrete system $L_{\Delta t,h}[v_{j,k}^{i+1}] = q_{j,k}^{i+1}$ has a unique solution $v_{j,k}^{i+1}$, $(x_j,y_k) \in N^0$ for any discrete right-hand side function $q_{j,k}^{i+1}$, $(x_j,y_k) \in M^0$.

REMARK 3.3. The solution of the (AP) (3.16)–(3.17) defines a discrete Green's operator $G_{\Delta t}^h$. Although the choice of boundary conditions (3.17) will affect the operator $G_{\Delta t}^h$, and thus the difference potentials and the projections defined below, it will not affect the resulting approximate solution to (3.1)–(3.3), as long as the (AP) is uniquely solvable and well-posed.

Construction of a Particular Solution: Let us denote by $u_{j,k}^{i+1} := G_{\Delta t}^h F_{j,k}^{i+1}$, $(x_j,y_k) \in N^+$ the particular solution of the discrete problem (3.9), which we will construct as the solution (restricted to set N^+) of the auxiliary problem (AP) (3.16)–(3.17) of the following form:

$$L_{\Delta t,h}[u_{j,k}^{i+1}] = \begin{cases} F_{j,k}^{i+1}, & (x_j,y_k) \in M^+, \\ 0, & (x_j,y_k) \in M^-, \end{cases} \tag{3.18}$$

$$u_{j,k}^{i+1} = 0, \quad (x_j,y_k) \in N^0 \backslash M^0 \tag{3.19}$$

The Difference Potential: We now introduce a linear space $\mathbf{V}_\gamma$ of all the grid functions denoted by v_γ^{i+1} defined on γ, similar to [3,41], etc. We will extend the value v_γ^{i+1} by zero to other points of the grid N^0.

DEFINITION 3.2. *The Difference Potential with any given density $v_\gamma^{i+1} \in \mathbf{V}_\gamma$ is the grid function $u_{j,k}^{i+1} := \mathbf{P}_{N^+\gamma} v_\gamma^{i+1}$, defined on N^+, and coincides on N^+ with the solution $u_{j,k}^{i+1}$ of the auxiliary problem (AP) (3.16)–(3.17) of the following form:*

$$L_{\Delta t,h}[u_{j,k}^{i+1}] = \begin{cases} 0, & (x_j, y_k) \in M^+, \\ L_{\Delta t,h}[v_\gamma^{i+1}], & (x_j, y_k) \in M^-, \end{cases} \tag{3.20}$$

$$u_{j,k}^{i+1} = 0, \quad (x_j, y_k) \in N^0 \backslash M^0 \tag{3.21}$$

Here, $\mathbf{P}_{N^+\gamma}$ denotes the operator which constructs the difference potential $u_{j,k}^{i+1} = \mathbf{P}_{N^+\gamma} v_\gamma^{i+1}$ from the given density $v_\gamma^{i+1} \in \mathbf{V}_\gamma$. The operator $\mathbf{P}_{N^+\gamma}$ is the linear operator of the density v_γ^{i+1}: $u_m^{i+1} = \sum_{l \in \gamma} A_{lm} v_l^{i+1}$, where $m \equiv (j,k)$ is the index of the grid point in the set N^+ and l is the index of the grid point in the set γ. Here, value u_m^{i+1} is the value of the difference potential $\mathbf{P}_{N^+\gamma} v_\gamma^{i+1}$ at time t^{i+1} at the grid point with an index $m : u_m = \mathbf{P}_{N^+\gamma} v_\gamma^{i+1}|_m$ and coefficients $\{A_{lm}\}$ are the coefficients of the difference potentials operator. The coefficients $\{A_{lm}\}$ can be computed by solving simple auxiliary problems (AP) (3.20)–(3.21) (or by constructing a difference potential operator) with the appropriate density v_γ^{i+1} defined at the points $(x_j, y_k) \in \gamma$.

Next, similarly to [3, 41], etc., we can define another operator $\mathbf{P}_\gamma : \mathbf{V}_\gamma \to \mathbf{V}_\gamma$ that is defined as the trace (or restriction/projection) of the difference potential $\mathbf{P}_{N^+\gamma} v_\gamma^{i+1}$ on the grid boundary γ:

$$\mathbf{P}_\gamma v_\gamma^{i+1} := Tr_\gamma(\mathbf{P}_{N^+\gamma} v_\gamma^{i+1}) = (\mathbf{P}_{N^+\gamma} v_\gamma^{i+1})|_\gamma \tag{3.22}$$

We will now formulate the crucial theorem of DPM (see, for example [3, 41], etc.).

THEOREM 3.1. *At each time level t^{i+1}, density u_γ^{i+1} is the trace of some solution u^{i+1} to the Difference Equations (3.9): $u_\gamma^{i+1} \equiv Tr_\gamma u^{i+1}$, if and only if, the following equality holds*

$$u_\gamma^{i+1} = \mathbf{P}_\gamma u_\gamma^{i+1} + G_{\Delta t}^h F_\gamma^{i+1}, \tag{3.23}$$

where $G_{\Delta t}^h F_\gamma^{i+1} := Tr_\gamma(G_{\Delta t}^h F^{i+1})$ is the trace of the particular solution $G_{\Delta t}^h F^{i+1}$ constructed in (3.18)–(3.19) on the grid boundary γ.

Proof. The proof follows closely the general argument from [41] and can be found, for example, in [3] (the extension to higher-dimensions is straightforward). ∎

REMARK 3.4.

(1) Note that at each time level t^{i+1}, the difference potential $\mathbf{P}_{N^+\gamma} u_\gamma^{i+1}$ is the solution to the homogeneous difference equation $L_{\Delta t,h}[u_{j,k}^{i+1}] = 0, (x_j, y_k) \in M^+$, and is uniquely defined once we know the value of the density u_γ^{i+1} at the points of the discrete grid boundary γ.

(2) Note that at each time level t^{i+1} the density u_γ^{i+1} has to satisfy the *Discrete Boundary Equations with Projection,* $u_\gamma^{i+1} - \mathbf{P}_\gamma u_\gamma^{i+1} = G_{\Delta t}^h F_\gamma^{i+1}$ in order to be a trace of the solution to the difference equation $L_{\Delta t,h}[u_{j,k}^{i+1}] = F_{j,k}^{i+1}, (x_j, y_k) \in M^+$.

Coupling of the Boundary Equations with Boundary Conditions: At each time level t^{i+1}, the discrete *Boundary Equations with Projections (3.23)* can be rewritten in a slightly different form as:

$$(\mathbf{I} - \mathbf{P}_\gamma) u_\gamma^{i+1} = G_{\Delta t}^h F_\gamma^{i+1}, \tag{3.24}$$

and is the linear system of equations for the unknown density u_γ^{i+1}. Here, $\mathbf{I}$ is the identity operator, $\mathbf{P}_\gamma$ is the projection operator, and the known right-hand side $G^h_{\Delta t}F_\gamma^{i+1}$ is the trace of the particular solution (3.18) on the discrete grid boundary γ.

The above system of discrete *Boundary Equations with Projection* (3.24) will have multiple solutions without boundary conditions (3.2), since it is equivalent to the difference equations $L_{\Delta t,h}[u_{j,k}^{i+1}]=F_{j,k}^{i+1},(x_j,y_k)\in M^+$. At each time level t^{i+1}, we need to supplement it by the boundary conditions (3.2) to construct the unique density $u_\gamma^{i+1}(x,y)\approx u(x,y,t^{i+1})$, where $u(x,y,t^{i+1})$ is the solution at $(x,y)\in\gamma$ at time t^{i+1} to the continuous model (3.1)–(3.3) and $u_\gamma^{i+1}(x,y)$ is the corresponding value of the discrete density.

Thus, we will consider the following approach to solve for the unknown density u_γ^{i+1} from the discrete *Boundary Equations with Projections* (3.24). At each time level t^{i+1}, one can represent the unknown densities u_γ^{i+1} through the values of the continuous solution and its gradients at the boundary of the domain with the desired accuracy: in other words, one can define a smooth extension operator for the solution of (3.1) from the continuous boundary $\Gamma=\partial\Omega$ to the discrete boundary γ. Note that the extension operator (the way it is constructed in this work) depends only on the properties of the given model and only uses the Cauchy data of the solution at the continuous boundary Γ.

For example, the extension operator of u_Γ^{i+1} from Γ to γ at time t^{i+1} can be defined according to the following 3-term Taylor formula:

$$\pi_{\gamma\Gamma}[\mathrm{u}_\Gamma^{i+1}]|_{(x_j,y_k)}\equiv u_{j,k}^{i+1}:=u|_\Gamma+d\frac{\partial u}{\partial n}\Big|_\Gamma+\frac{d^2}{2!}\frac{\partial^2 u}{\partial n^2}\Big|_\Gamma,\quad (x_j,y_k)\in\gamma, \tag{3.25}$$

where $\pi_{\gamma\Gamma}[\mathrm{u}_\Gamma^{i+1}]$ defines the smooth extension operator of Cauchy data $\mathrm{u}_\Gamma^{i+1}:=\left(u(x,y,t^{i+1})\Big|_\Gamma,\frac{\partial u}{\partial n}(x,y,t^{i+1})\Big|_\Gamma\right)$ at t^{i+1} from the continuous boundary Γ to the discrete boundary γ, and d denotes the signed distance from the point $(x_j,y_k)\in\gamma$ to the nearest boundary point on the continuous boundary Γ of the domain Ω (the signed length of the shortest normal from the point $(x_j,y_k)\in\gamma$ to the point on the continuous boundary Γ of the domain Ω). We take the signed distance either with sign "+" (if the point $(x_j,y_k)\in\gamma$ is outside of the domain Ω), or with sign "−" (if the point $(x_j,y_k)\in\gamma$ is inside the domain Ω). The choice of a 3–term extension operator (3.25) is sufficient for the second-order method based on Difference Potentials (see numerical tests in Section 6).

For example, the extension operator of u_Γ^{i+1} from Γ to γ at time t^{i+1} can also be defined according to the following 5-term Taylor formula:

$$\pi_{\gamma\Gamma}[\mathrm{u}_\Gamma^{i+1}]|_{(x_j,y_k)}\equiv u_{j,k}^{i+1}:=u|_\Gamma+d\frac{\partial u}{\partial n}\Big|_\Gamma+\frac{d^2}{2!}\frac{\partial^2 u}{\partial n^2}\Big|_\Gamma+\frac{d^3}{3!}\frac{\partial^3 u}{\partial n^3}\Big|_\Gamma+\frac{d^4}{4!}\frac{\partial^4 u}{\partial n^4}\Big|_\Gamma,\quad (x_j,y_k)\in\gamma, \tag{3.26}$$

again, as in (3.25), $\pi_{\gamma\Gamma}[\mathrm{u}_\Gamma^{i+1}]$ defines the smooth extension operator of the Cauchy data $\mathrm{u}_\Gamma^{i+1}:=\left(u(x,y,t^{i+1})\Big|_\Gamma,\frac{\partial u}{\partial n}(x,y,t^{i+1})\Big|_\Gamma\right)$ at t^{i+1} from the continuous boundary Γ to the discrete boundary γ, d denotes the signed distance from the point $(x_j,y_k)\in\gamma$ to the nearest boundary point on the continuous boundary Γ of the domain Ω. As before, we take it either with sign "+" (if the point $(x_j,y_k)\in\gamma$ is outside of the domain Ω), or with sign "−" (if the point $(x_j,y_k)\in\gamma$ is inside the domain Ω). The choice of a 5–term extension operator (3.26) is sufficient for the fourth-order method based on Difference Potentials, see Section 6. To simplify the formulas in (3.25) and (3.26), we employed

the following notations:

$$u|_\Gamma := u(x,y,t^{i+1})|_\Gamma, \qquad \frac{\partial u}{\partial n}\Big|_\Gamma := \frac{\partial u}{\partial n}(x,y,t^{i+1})\Big|_\Gamma, \qquad \frac{\partial^2 u}{\partial n^2}\Big|_\Gamma := \frac{\partial^2 u}{\partial n^2}(x,y,t^{i+1})\Big|_\Gamma,$$

$$\frac{\partial^3 u}{\partial n^3}\Big|_\Gamma := \frac{\partial^3 u}{\partial n^3}(x,y,t^{i+1})\Big|_\Gamma, \qquad \frac{\partial^4 u}{\partial n^4}\Big|_\Gamma := \frac{\partial^4 u}{\partial n^4}(x,y,t^{i+1})\Big|_\Gamma,$$

where $(x,y)\in\Gamma$ denotes the nearest point to $(x_j,y_k)\in\gamma$.

Next, at the fixed time level t^{i+1}, for any sufficiently smooth single-valued periodic function $g(\vartheta,t^{i+1})$ on Γ with a period $|\Gamma|$, assume that the sequence denoted by $\varepsilon_{\mathcal{N}^0,\mathcal{N}^1}$ and defined as

$$\varepsilon_{\mathcal{N}^0,\mathcal{N}^1} = \min_{c_\nu^{0,i+1},c_\nu^{1,i+1}} \int_\Gamma \Big(|g(\vartheta,\cdot) - \sum_{\nu=0}^{\mathcal{N}^0} c_\nu^{0,i+1}\phi_\nu^0(\vartheta)|^2 + |g'(\vartheta,\cdot) - \sum_{\nu=0}^{\mathcal{N}^1} c_\nu^{1,i+1}\phi_\nu^1(\vartheta)|^2\Big)\mathrm{d}\vartheta \tag{3.27}$$

tends to zero with increasing number $\mathcal{N}^0$ and $\mathcal{N}^1$ of basis functions: $\lim \varepsilon_{\mathcal{N}^0,\mathcal{N}^1} = 0$ as $\mathcal{N}^0\to\infty$, $\mathcal{N}^1\to\infty$. Here, functions $(\phi_\nu^0(\vartheta),\phi_\nu^1(\vartheta))$ are the selected set of basis functions defined on the boundary of the domain Γ and real numbers $(c_\nu^{0,i+1},c_\nu^{1,i+1})$, $(\nu = 0,1,...,\mathcal{N}^0,\nu=0,1,...,\mathcal{N}^1)$ are the expansion coefficients in front of the basis functions at time level t^{i+1}. The parameter ϑ can be thought of as the arc length along Γ, and $|\Gamma|$ is the length of the boundary. We selected arc length ϑ at this point only for the sake of definiteness. Other parametrizations along Γ are used in the numerical examples (Γ is defined using polar coordinates for the circular domain and is defined using elliptical coordinates for the elliptical domain), see Section 6 and the brief discussion in the Appendix Section 7. In particular, in the Appendix Section 7 we give details of the construction of the extension operators (3.25) and (3.26) using the continuous PDE model (3.1) and the knowledge of the Cauchy data u_Γ^{i+1}.

Therefore, at every time level t^{i+1}, to discretize the elements $\mathrm{u}_\Gamma^{i+1} \equiv \Big(u(\vartheta,t^{i+1}),\frac{\partial u}{\partial n}(\vartheta,t^{i+1})\Big)$, $\vartheta\in\Gamma$ from the space of Cauchy data, one can use the approximate equalities:

$$\tilde{\mathrm{u}}_\Gamma^{i+1} = \sum_{\nu=0}^{\mathcal{N}^0} c_\nu^{0,i+1}\Phi_\nu^0(\vartheta) + \sum_{\nu=0}^{\mathcal{N}^1} c_\nu^{1,i+1}\Phi_\nu^1(\vartheta), \quad \tilde{\mathrm{u}}_\Gamma^{i+1} \approx \mathrm{u}_\Gamma^{i+1} \tag{3.28}$$

where $\Phi_\nu^0 = (\phi_\nu^0,0)$ and $\Phi_\nu^1 = (0,\phi_\nu^1)$ are the set of basis functions used to represent the Cauchy data on the boundary of the domain Γ, and real numbers $(c_\nu^{0,i+1},c_\nu^{1,i+1})$ with $(\nu=0,1,...,\mathcal{N}^0,\nu=0,1,...,\mathcal{N}^1)$ are the unknown numerical coefficients to be determined at every time level t^{i+1}.

Remark 3.5. For smooth Cauchy data, it is expected that a relatively small number $(\mathcal{N}^0,\mathcal{N}^1)$ of basis functions are required to approximate the Cauchy data of the unknown solution at time level t^{i+1}, due to the rapid convergence of the expansions (3.28). Hence, in practice, we use a relatively small number of basis functions in (3.28), which leads to a very efficient numerical algorithm based on the Difference Potentials approach, see Section 6.

In the case of the Dirichlet boundary condition in (3.1)–(3.3), $u(\vartheta,t^{i+1}),\vartheta\in\Gamma$ is known. Hence, at every time level t^{i+1} the coefficients $c_\nu^{0,i+1}$ in (3.28) are given as the data that can be determined as the minimization of $\int_\Gamma |u(\vartheta,t^{i+1}) - \sum_{\nu=0}^{\mathcal{N}^0} c_\nu^{0,i+1}\phi_\nu^0|^2\mathrm{d}\vartheta$. For other boundary value problems (3.1), the procedure is similar to the case presented

for Dirichlet data. For example, in the case of Neumann boundary condition in (3.2), at every t^{i+1} the coefficients $c_\nu^{1,i+1}$ in (3.28) are known and again found as the minimization of $\int_\Gamma |\frac{\partial u}{\partial n}(\vartheta,t^{i+1}) - \sum_{\nu=0}^{\mathcal{N}^1} c_\nu^{1,i+1}\phi_\nu^1|^2 \mathrm{d}\vartheta$.

After the selection of the parametrization ϑ of Γ and construction of the extension operator, we use spectral approximation (3.28) in the extension operator $u_\gamma^{i+1} = \pi_{\gamma\Gamma}[\tilde{u}_\Gamma^{i+1}]$:

$$u_\gamma^{i+1} = \sum_{\nu=0}^{\mathcal{N}^0} c_\nu^{0,i+1}\pi_{\gamma\Gamma}[\Phi_\nu^0(\vartheta)] + \sum_{\nu=0}^{\mathcal{N}^1} c_\nu^{1,i+1}\pi_{\gamma\Gamma}[\Phi_\nu^1(\vartheta)]. \tag{3.29}$$

Therefore, at every time level t^{i+1}, boundary equations (BEP) (3.24) becomes an overdetermined linear system of dimension $|\gamma| \times (\mathcal{N}^0 + \mathcal{N}^1)$ for the unknowns $(c_\nu^{0,i+1}, c_\nu^{1,i+1})$ (note that in general it is assumed that $|\gamma| >> (\mathcal{N}^0 + \mathcal{N}^1)$). This system (3.24) for $(c_\nu^{0,i+1}, c_\nu^{1,i+1})$ is solved using the least-squares method, and hence one obtains the unknown density u_γ^{i+1}.

The final step of the DPM is to use the computed density u_γ^{i+1} to construct the approximation to the solution (3.1)–(3.3) inside the physical domain Ω.

Generalized Green's Formula:

STATEMENT 3.1. *The discrete solution* $u_{j,k}^{i+1} := \mathbf{P}_{N^+\gamma} u_\gamma^{i+1} + G_{\Delta t}^h F^{i+1}, (x_j, y_k) \in N^+$ *at each time* t^{i+1} *is the approximation to the exact solution* $u(x_j, y_k, t^{i+1})$, $(x_j, y_k) \in N^+ \cap \bar{\Omega}$, $t^{i+1} \in (0, T]$ *of the continuous problem (3.1)–(3.3).*

Discussion: Note, as the first step of the developed high-order accurate methods based on Difference Potentials, we reformulate the original continuous models (3.1) in the time-discrete form (3.7)–(3.8) using accurate and stable schemes. Hence, we develop high-order accurate Difference Potentials methods for (3.1)–(3.3) by employing the elliptic structure of the continuous models. Furthermore, note that once density $u_\gamma^{i+1} \in \mathbf{V}_\gamma$ is obtained with high-order accuracy from the *Boundary Equations with Projection* (3.24): $(\mathbf{I} - \mathbf{P}_\gamma) u_\gamma^{i+1} = G_{\Delta t}^h F_\gamma^{i+1}, (x_j, y_k) \in \gamma$, the problem of finding accurate approximation $u_{j,k}^{i+1} \equiv \mathbf{P}_{N^+\gamma} u_\gamma^{i+1} + G_{\Delta t}^h F^{i+1}, (x_j, y_k) \in N^+$ at each time t^{i+1} to the solution $u(x_j, y_k, t^{i+1})$ of the continuous problem (3.1)–(3.3) reduces to the solution of a simple auxiliary problem on a computationally simple auxiliary domain Ω^0 (for example, Ω^0 can be a square):

The approximate solution $u_{j,k}^{i+1} \equiv \mathbf{P}_{N^+\gamma} u_\gamma^{i+1} + G_{\Delta t}^h F^{i+1}, (x_j, y_k) \in N^+$ at time t^{i+1} coincides on N^+ with the solution of the following simple auxiliary problem:

$$L_{\Delta t,h}[u_{j,k}^{i+1}] = \begin{cases} F_{j,k}^{i+1}, & \forall (x_j, y_k) \in M^+, \\ \\ L_{\Delta t,h}[u_\gamma^{i+1}], & \forall (x_j, y_k) \in M^-, \end{cases} \tag{3.30}$$

subject to the boundary conditions:

$$u_{j,k}^{i+1} = 0, \quad \forall (x_j, y_k) \in N^0 \backslash M^0.$$

Thus, the result of the above Statement 3.1 is the consequence of the sufficient regularity of the exact solution (and domain), Theorem 3.1, the result of the extension operator (3.25) or (3.26), as well as the second-order and the fourth-order accuracy of the underlying discretization (3.9) and the established convergence results and error estimates for the Difference Potentials Method for general linear elliptic boundary value

problems in arbitrary domains with sufficiently smooth boundaries [16, 35, 36, 41]. In particular, we can recall, that in [35,36] it was shown (under sufficient regularity of the exact solution and considered domain), that the Difference Potentials approximate surface potentials of the elliptic operators (and, therefore DPM approximates the solution to the elliptic boundary value problem) with the accuracy of $O(h^{\mathcal{P}-\varepsilon})$ in the discrete Hölder norm of order $\mathcal{Q}+\varepsilon$. Here, $0<\varepsilon<1$ is an arbitrary number, $\mathcal{Q}$ is the order of the considered elliptic operator (in the current work, $\mathcal{Q}=2$), and $\mathcal{P}$ is the order of the scheme used for the approximation of the elliptic operator (in this work, we have $\mathcal{P}=2$, if the second-order scheme is considered for the approximation of the elliptic operator, or $\mathcal{P}=4$, if the fourth-order scheme is used for the approximation of the elliptic operator). Readers can consult [35,36] or [41] for the details and proof of the general result.

Therefore, in this work, for sufficiently small enough h and Δt, we expect that at every time level t^{i+1} the constructed discrete solution $u^{i+1}_{j,k}=\mathbf{P}_{N^+\gamma}u^{i+1}_{\gamma}+G^h_{\Delta t}F^{i+1}$ will approximate the exact solution, $u^{i+1}_{j,k}\approx u(x_j,y_k,t^{i+1})$, $(x_j,y_k)\in N^+\cap\bar{\Omega}$, $t^{i+1}\in(0,T]$ of the continuous problem (3.1)–(3.3), with $O(h^2+\Delta t^2)$ for DPM2 and with $O(h^4+\Delta t^4)$ for DPM4 in the maximum norm.

Remark 3.6.

(1) The formula $\mathbf{P}_{N^+\gamma}u^{i+1}_{\gamma}+G^h_{\Delta t}F^{i+1}$ is the *discrete generalized Green's formula.*

(2) Note that, at each time level t^{i+1}, after the density u^{i+1}_{γ} is reconstructed from the *Boundary Equations with Projection* (3.24), the Difference Potential is easily obtained as the solution of a simple (AP) using Def. 3.2.

4. Schemes based on difference potentials for interface and composite domains problems

In Section 3.1 we constructed second and fourth-order schemes based on Difference Potentials for problems in the single domain Ω. In this section, we will show how to extend these methods to interface/composite domains problems (2.1)–(2.7).

First, as we have done in Section 3.1 for the single domain Ω, we will introduce the auxiliary domains. We will place each of the original subdomains Ω_s in the auxiliary domains $\Omega^0_s\subset\mathbb{R}^2,(s=1,2)$ and will state the auxiliary difference problems in each subdomain $\Omega_s,(s=1,2)$. The choice of the auxiliary domains Ω^0_1 and Ω^0_2, as well as the auxiliary difference problems, may be made independently of each other. After that, for each subdomain, we will proceed in a similar way as we did in Section 3.1. Also, for each auxiliary domain Ω^0_s we will consider, for example a Cartesian mesh (the choice of the grids for the auxiliary problems will be independent of each other and the grids do not need to conform/align with the boundaries of the subdomains/interfaces). After that, all the definitions, notations, and properties introduced in Section 3.1 extend to each subdomain Ω_s in a direct way. As before, index $s,(s=1,2)$ is used to distinguish between each subdomain. Let us denote the discrete version of the problem (2.1)–(2.7) for each subdomain as:

$$L^s_{\Delta t,h}[u^{i+1}_{j,k}]=F_s{}^{i+1}_{j,k},\quad (x_j,y_k)\in M^+_s, \tag{4.1}$$

The difference problem (4.1) is obtained using either the second-order or the fourth-order underlying discretization (3.9). The main theorem of the method for the composite domains/interface problems is given below.

Statement 4.1.

At each time level t^{i+1}, density $u^{i+1}_{\gamma}:=(u^{i+1}_{\gamma_1},u^{i+1}_{\gamma_2})$ is the trace of some solution u^{i+1} on $\Omega_1\cup\Omega_2$ to the Difference Equations (4.1): $u^{i+1}_{\gamma}\equiv Tr_{\gamma}u^{i+1}$, if and only if, the

following equalities hold

$$u^{i+1}_{\gamma_1} = \mathbf{P}_{\gamma_1} u^{i+1}_{\gamma_1} + G^h_{\Delta t} F^{i+1}_{\gamma_1}, (x_j, y_k) \in \gamma_1 \tag{4.2}$$

$$u^{i+1}_{\gamma_2} = \mathbf{P}_{\gamma_2} u^{i+1}_{\gamma_2} + G^h_{\Delta t} F^{i+1}_{\gamma_2}, (x_j, y_k) \in \gamma_2 \tag{4.3}$$

The obtained discrete solution $u^{i+1}_{j,k} := \mathbf{P}_{\mathbf{s}\, N^+_s \gamma_s} u^{i+1}_{\gamma_s} + G^h_{s\, \Delta t} F^{i+1}_s, (x_j, y_k) \in N^+_s$ *at each* t^{i+1} *is the approximation to the exact solution* $u(x_j, y_k, t^{i+1})$, $(x_j, y_k) \in N^+_s \cap \bar{\Omega}_s$, $t^{i+1} \in (0, T]$ *of the continuous model problem (2.1)–(2.7). Here, index* $s = 1, 2$.

Discussion: The result is a consequence of the results in Section 3.1. We expect that at every time level t^{i+1}, the solution $u^{i+1}_{j,k} = \mathbf{P}_{\mathbf{s}\, N^+_s \gamma_s} u^{i+1}_{\gamma_s} + G^h_{s\, \Delta t} F^{i+1}_s, (x_j, y_k) \in N^+_s$ will approximate the exact solution $u(x_j, y_k, t^{i+1})$, $(x_j, y_k) \in N^+_s \cap \bar{\Omega}_s$, $t^{i+1} \in (0, T]$, $(s = 1, 2)$, with the accuracy $O(h^2 + \Delta t^2)$ for the second-order method DPM2, and with the accuracy $O(h^4 + \Delta t^4)$ for the fourth-order method DPM4 in the maximum norm. Moreover, as we observed in the numerical experiments in Section 6 (see also [2, 3, 12]), the same high-order accuracy is preserved in the approximate gradient of the solution. See Section 6 for the extensive numerical results.

REMARK 4.1. Similar to the discussion in Section 3.1, at each time t^{i+1}, the *Boundary Equations* (4.2)–(4.3) are coupled with boundary (2.5) and interface/matching conditions (2.3)–(2.4) to obtain the unique densities $u^{i+1}_{\gamma_1}$ and $u^{i+1}_{\gamma_2}$. We consider the same extension formula (3.25) (for the second-order method) or (3.26) (for the fourth-order method) to construct $u^{i+1}_{\gamma_s}, s = 1, 2$ in each subdomain/domain.

5. Numerical algorithm

In this section we will briefly summarize the main steps of the algorithm for the reader's convenience:

Step 1: Introduce a computationally simple auxiliary domain and formulate the auxiliary problem (AP).

Step 2: At each time t^{i+1} compute a *Particular Solution*, $u^{i+1}_{j,k} = G^h_{\Delta t} F^{i+1}_{j,k}, (x_j, y_k) \in N^+$, as the solution of the (AP). For the single domain method, see (3.18)–(3.19) in Section 3.1 (DPM2 and DPM4). For the direct extension of the algorithms to interface and composite domains problems, see Section 4.

Step 3: Next, at each time level t^{i+1} compute the unknown *boundary values or densities*, $u^{i+1}_{\gamma} \in \mathbf{V}_{\gamma}$ at the points of the *discrete grid boundary* γ by solving the system of linear equations derived from the system of *Boundary Equations with Projection combined with the extension operator for the density*: see (3.24) and (3.29) in Section 3.1, and extension to interface and composite domain problems (4.2)–(4.3) in Section 4.

REMARK 5.1. Note, that the computation of the matrix for the system of *Boundary Equations with Projection* (3.24) is the key contribution to the overall computational complexity of the algorithm. However, if the time step Δt is kept constant, then the matrix associated with the system of *Boundary Equations with Projection* (3.24) can be computed only once at initial time step and stored. Thus, only the right-hand side will be updated at each time level t^{i+1} in the linear system of *Boundary Equations with Projection* (3.24). Therefore, the computations at each time level t^{i+1} will be performed very efficiently.

Step 4: Using the definition of the Difference Potential, Def. 3.2, Section 3.1, and Section 4 (algorithm for interface/composite domain problems), construct the *Difference Potential,* $\mathbf{P}_{N^+\gamma} u^{i+1}_{\gamma}$ from the obtained density, u^{i+1}_{γ}.

Step 5: Finally, at each time t^{i+1}, reconstruct the approximation to the continuous solution from u_γ^{i+1} using the generalized Green's formula, $u(x_j,y_k,t^{i+1}) \approx \mathbf{P}_{N^+\gamma} u_\gamma^{i+1} + G^h_{\Delta t} F^{i+1}, (x_j,y_k) \in N^+$, see Statement 3.1 in Section 3.1, and see Statement 4.1 in Section 4 (algorithm for interface/composite domain problems).

6. Numerical tests

In this section, we present several numerical experiments for interface/composite domain problems that illustrate the high-order accuracy and efficiency of the methods based on Difference Potentials presented in Sections 3.1–5.

In all the numerical tests below, similar to our work in 1D [3], the error in the approximation to the exact solution of the model is determined by the size of the maximum error up to the interface in both subdomains Ω_1 and Ω_2, Figure 2.1:

$$E := \max_{t^i \in [0,T]} \max_{(x_j,y_k) \in M_1^+ \cup M_2^+} |u(x_j,y_k,t^i) - u^i_{j,k}|, \tag{6.1}$$

where $u(x_j,y_k,t^i)$ denotes the exact solution to the continuous model (2.1)–(2.7), $u^i_{j,k}$ denotes the numerical approximation at time t^i at mesh node (x_j,y_k), and M_1^+ and M_2^+ are the sets of the interior mesh nodes for the subdomain Ω_1 and Ω_2, respectively. Moreover, similar to [3] we also compute the maximum error of the components of the discrete gradient up to the interface in both subdomains Ω_1 and Ω_2, which are determined by the following centered difference formulas:

$$E_{\nabla_x} := \max_{t^i \in [0,T]} \max_{(x_j,y_k) \in M_1^+ \cup M_2^+} |\nabla_x u^i - \nabla_x u^i_{j,k}|, \tag{6.2}$$

$$E_{\nabla_y} := \max_{t^i \in [0,T]} \max_{(x_j,y_k) \in M_1^+ \cup M_2^+} |\nabla_y u^i - \nabla_y u^i_{j,k}|, \tag{6.3}$$

where

$$\nabla_x u^i - \nabla_x u^i_{j,k} := \frac{u(x_j+h,y_k,t^i) - u(x_j-h,y_k,t^i)}{2h} - \frac{u^i_{j+1,k} - u^i_{j-1,k}}{2h},$$

and

$$\nabla_y u^i - \nabla_y u^i_{j,k} := \frac{u(x_j,y_k+h,t^i) - u(x_j,y_k-h,t^i)}{2h} - \frac{u^i_{j,k+1} - u^i_{j,k-1}}{2h}.$$

Remark 6.1.

(1) Similar to [2], below in Section 6.1 we consider interface/composite domain problems defined in domains similar to the example of the domains Ω_1 and Ω_2 illustrated on Figure 2.1, Section 2. Thus, for the exterior domain Ω_1 we select auxiliary domain Ω_1^0 to be a rectangle with the boundary $\partial\Omega_1^0$, which coincides with the exterior boundary $\partial\Omega_1$ of the domain Ω_1. After that, we construct methods based on Difference Potentials as presented in Sections 3.1–5. To take advantage of the given boundary conditions, for example, Dirichlet boundary conditions and specifics of the exterior domain Ω_1/auxiliary domain Ω_1^0, for the *fourth-order method DPM4* we construct the particular solution (3.18) and Difference Potential (3.20) for the exterior auxiliary problem in Ω_1^0 using the discrete operator $L^1_{\Delta t,h}[u^{i+1}_{j,k}]$ (see (3.9)–(3.10) and (3.15)) with a modified stencil near the boundary of the auxiliary domain Ω_1^0 as follows (example of the point at "southwest" corner of the grid):

$$L^1_{\Delta t,h}[u^{i+1}_{1,1}] := \frac{10u^{i+1}_{0,1} - 15u^{i+1}_{1,1} - 4u^{i+1}_{2,1} + 14u^{i+1}_{3,1} - 6u^{i+1}_{4,1} + u^{i+1}_{5,1}}{12h^2}$$

$$+\frac{10u_{1,0}^{i+1}-15u_{1,1}^{i+1}-4u_{1,2}^{i+1}+14u_{1,3}^{i+1}-6u_{1,4}^{i+1}+u_{1,5}^{i+1}}{12h^2}-\sigma_1^2u_{1,1}^{i+1},\ \text{in}\ \Omega_1^0. \tag{6.4}$$

Other near-boundary nodes in Ω_1^0 are handled in a similar way in $L^1_{\Delta t,h}[u_{j,k}^{i+1}]$ in (3.15) (fourth-order scheme). Similarly, one can incorporate, mixed boundary conditions (Dirichlet and Neumann boundary conditions as in Table 6.5) into the particular solution (3.18) and Difference Potential (3.20) of the exterior auxiliary problem in Ω_1^0 for DPM4.

Note, that to construct a particular solution (3.18) and Difference Potential (3.20) for the interior problem stated in auxiliary domain Ω_2^0, we do not modify the stencil in $L_h[u_{j,k}^{i+1}]$ in (3.15) (fourth-order scheme) near the boundary $\partial\Omega_2^0$ of the interior auxiliary domain Ω_2^0. For the second-order method DPM2 (see (3.9)–(3.10) and (3.13)), we also take advantage of the given boundary conditions and specifics of the exterior domain Ω_1/auxiliary domain Ω_1^0 in the construction of the the particular solution (3.18) and the Difference Potential (3.20) for the exterior auxiliary problem in Ω_1^0. However, there is no need for the modification of the stencil (we just replace zero boundary conditions in (3.18)–(3.19) and in (3.20)–(3.21) by the given boundary conditions on the boundary of $\partial\Omega_1\equiv\partial\Omega_1^0$.)

(2) In all numerical tests in Section 6.1, we select a standard trigonometric system of basis functions for the spectral approximation in (3.28), Section 3.1: $\phi_0(\vartheta)=1$, $\phi_1(\vartheta)=\sin\left(\frac{2\pi}{|\Gamma|}\vartheta\right)$, $\phi_2(\vartheta)=\cos\left(\frac{2\pi}{|\Gamma|}\vartheta\right)$, …, $\phi_{2\nu}(\vartheta)=\cos\left(\frac{2\pi\nu}{|\Gamma|}\vartheta\right)$ and $\phi_{2\nu+1}(\vartheta)=\sin\left(\frac{2\pi\nu}{|\Gamma|}\vartheta\right),\nu=0,1,2,\ldots$. Here, $\phi_\nu\equiv\phi_\nu^0\equiv\phi_\nu^1$. Also, note that, in the tests in Section 6.1, we denote by $\mathcal{N}_1^0+\mathcal{N}_1^1$ the total number of harmonics that is used to approximate the Cauchy data in (3.28) if we consider unknowns from subdomain Ω_1 as the independent unknowns, or we denote by $\mathcal{N}_2^0+\mathcal{N}_2^1$ the total number of harmonics that is used to approximate the Cauchy data in (3.28) if we consider unknowns from subdomain Ω_2 as the independent unknowns in (3.28) (see interface conditions (2.3)–(2.4)).

6.1. Second-order DPM2 and fourth-order DPM4: numerical results. In this section we consider parabolic composite domain/interface models of the form (2.1)–(2.2). On several challenging tests below, we numerically verify expected convergence rates $O(\Delta t^2+h^2)$ for DPM2 and $O(\Delta t^4+h^4)$ for DPM4.

In particular, we consider here the following example of the parabolic interface/composite domains models:

$$\frac{\partial u_{\Omega_s}}{\partial t}-\nabla\cdot(\lambda_s\nabla u_{\Omega_s})=f_s(x,y,t),\quad s=1,2 \tag{6.5}$$

subject to the interface and boundary conditions in the form of (2.3)–(2.5), and initial conditions of the form (2.6)–(2.7). Interface conditions for the numerical tests are computed using the exact solutions $u(x,y,t)$, and the boundary condition on $\partial\Omega_1$ is obtained from the Dirichlet boundary condition of the exact solution $u(x,y,t)$ on the boundary of the exterior domain $\partial\Omega_1$ for all the tests except for the test in Table 6.5. To illustrate the performance of the proposed methods on different boundary conditions, in Table 6.5 we consider the mixed boundary conditions (Dirichlet and Neumann boundary conditions) on the boundary of the exterior domain $\partial\Omega_1$. Again, these boundary conditions are obtained from the Dirichlet and Neumann boundary conditions of the exact solution $u(x,y,t)$. Finally, the initial conditions are obtained using the exact solution $u(x,y,0)$ at time $t=0$.

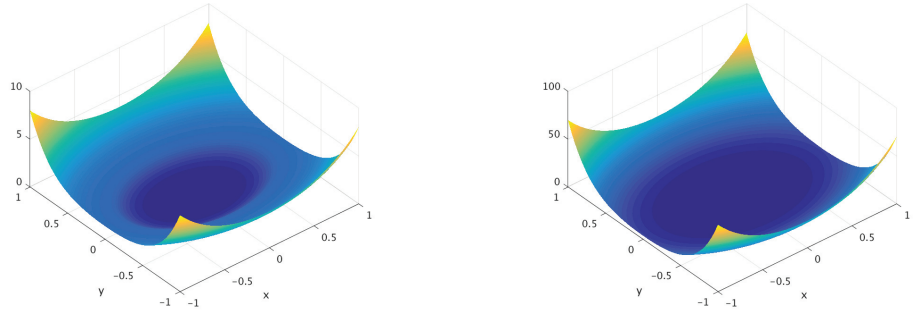

FIG. 6.1. *Example of the solution (6.7) with interface defined by* $\Gamma: x^2/(\pi^2/16)+y^2/(\pi^2/36)=1$ *(left figure) and example of the solution (6.8) with interface defined by* $\Gamma: x^2/(\pi^2/16)+y^2/(\pi^2/36)=1$ *(right figure). The solutions are obtained by BDF4-DPM4 on grid* 1280×1280 *at a final time* $T=0.1$. *Model (6.5) with* $\lambda_1=10,\lambda_2=1$ *is used for both figures.*

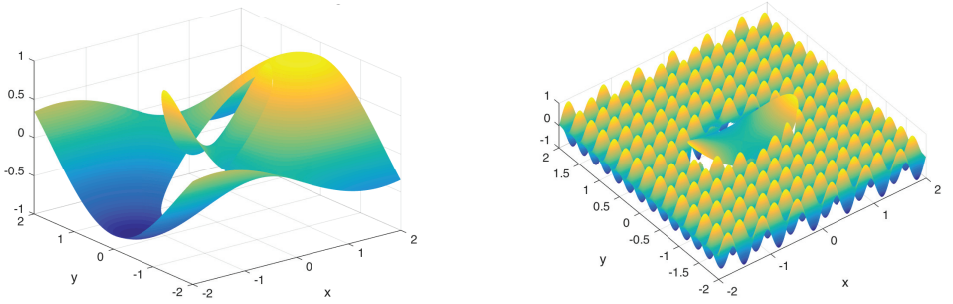

FIG. 6.2. *Example of the solution (6.9) with interface defined by* $\Gamma: x^2+4y^2=1$ *(left figure) and example of the solution (6.10) with interface defined by* $\Gamma: x^2+4y^2=1$ *(right figure). The solutions are obtained by BDF4-DPM4 on grid* 1280×1280 *at a final time* $T=0.1$. *Model (6.5) with* $\lambda_1=\lambda_2=1$ *is used for both figures.*

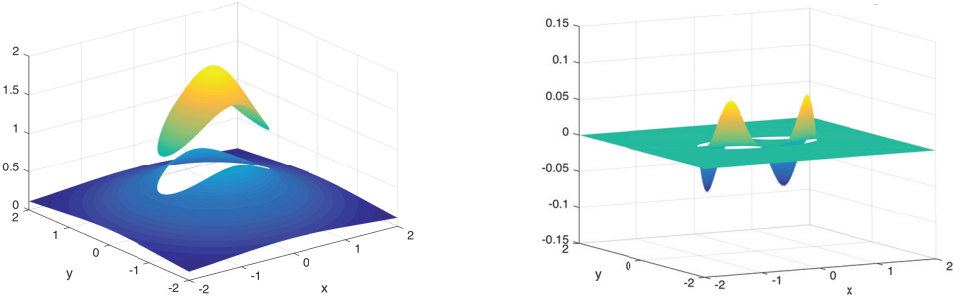

FIG. 6.3. *Example of the solution (6.11) with interface defined by* $\Gamma: x^2+4y^2=1$ *(left figure) and example of the solution (6.12) with interface defined by* $\Gamma: x^2+4y^2=1$. *The solutions are obtained by BDF4-DPM4 on grid* 1280×1280 *at a final time* $T=0.1$. *Model (6.5) with* $\lambda_1=\lambda_2=1$ *is used for the left figure and model (6.5) with* $\lambda_1=1,\lambda_2=1000$ *is used for the right figure.*

Grid	E: DPM2	Rate	E: DPM4	Rate
80×80	3.0147 E−3	—	9.6646 E−6	—
160×160	7.6599 E−4	1.98	2.4457 E−7	5.30
320×320	1.9352 E−4	1.98	1.7783 E−8	3.78
640×640	4.8455 E−5	2.00	1.2139 E−9	3.87
1280×1280	1.2096 E−5	2.00	9.4707 E−11	3.68
Grid	$E_{\nabla x}$: DPM2	Rate	$E_{\nabla x}$: DPM4	Rate
80×80	1.8629 E−2	—	6.3170 E−5	—
160×160	5.3143 E−3	1.81	4.3396 E−6	3.86
320×320	1.2337 E−3	2.11	3.0004 E−7	3.85
640×640	3.1648 E−4	1.96	2.4113 E−8	3.64
1280×1280	8.7970 E−5	1.85	1.7743 E−9	3.76
Grid	$E_{\nabla y}$: DPM2	Rate	$E_{\nabla y}$: DPM4	Rate
80×80	2.5495 E−2	—	8.5030 E−5	—
160×160	6.0501 E−3	2.08	4.3380 E−6	4.29
320×320	2.1026 E−3	1.52	4.0019 E−7	3.44
640×640	5.1200 E−4	2.04	2.5572 E−8	3.97
1280×1280	1.2032 E−4	2.09	1.7881 E−9	3.84

TABLE 6.1. *Grid convergence in the approximate solution and components of the discrete gradient for BDF2-DPM2 and BDF4-DPM4. The interior domain Ω_2 is the ellipse with $a=\pi/4, b=\pi/6$ centered at the origin, and the exterior domain is $\Omega_1=[-1,1]\times[-1,1]\backslash\Omega_2$. Test problem* (6.5), (6.7) *with continuous solution and continuous flux and material coefficients $\lambda_1=10, \lambda_2=1$. The dimension of the set of basis functions is $\mathcal{N}_1^0+\mathcal{N}_1^1=3$.*

Grid	E: DPM2	Rate	E: DPM4	Rate
80×80	2.0619 E−2	—	3.3646 E−5	—
160×160	4.7572 E−3	2.12	2.0364 E−6	4.05
320×320	1.1292 E−3	2.07	1.1834 E−7	4.11
640×640	2.7477 E−4	2.04	7.2672 E−9	4.03
1280×1280	6.9163 E−5	1.99	5.5669 E−10	3.71
Grid	$E_{\nabla x}$: DPM2	Rate	$E_{\nabla x}$: DPM4	Rate
80×80	5.2046 E−2	—	1.2772 E−4	—
160×160	1.4393 E−2	1.85	1.0497 E−5	3.60
320×320	4.0794 E−3	1.82	7.9414 E−7	3.72
640×640	1.0870 E−3	1.91	5.9797 E−8	3.73
1280×1280	2.8509 E−4	1.93	4.2368 E−9	3.82
Grid	$E_{\nabla y}$: DPM2	Rate	$E_{\nabla y}$: DPM4	Rate
80×80	6.9755 E−2	—	1.4278 E−4	—
160×160	1.9215 E−2	1.86	1.2204 E−5	3.55
320×320	5.1537 E−3	1.90	9.6832 E−7	3.66
640×640	1.3364 E−3	1.95	6.4240 E−8	3.91
1280×1280	3.5170 E−4	1.93	4.4682 E−9	3.85

TABLE 6.2. *Grid convergence in the approximate solution and components of the discrete gradient for BDF2-DPM2 and BDF4-DPM4. The interior domain Ω_2 is the ellipse with $a=\pi/4, b=\pi/6$ centered at the origin, and the exterior domain is $\Omega_1=[-1,1]\times[-1,1]\backslash\Omega_2$. Test problem* (6.5), (6.8) *with continuous solution and discontinuous flux and material coefficients $\lambda_1=10, \lambda_2=1$. The dimension of the set of basis functions is $\mathcal{N}_1^0+\mathcal{N}_1^1=3$.*

Grid	E: DPM2	Rate	E: DPM4	Rate
80×80	1.4960 E−5	—	7.6437 E−9	—
160×160	3.3252 E−6	2.17	2.6351 E−10	4.86
320×320	8.0747 E−7	2.04	1.5220 E−11	4.11
640×640	2.0550 E−7	1.97	1.0545 E−12	3.85
1280×1280	5.2287 E−8	1.97	5.0193 E−13	1.07
Grid	$E_{\nabla x}$: DPM2	Rate	$E_{\nabla x}$: DPM4	Rate
80×80	9.6755 E−5	—	2.3023 E−8	—
160×160	2.7633 E−5	1.81	1.0647 E−9	4.43
320×320	7.3440 E−6	1.91	7.2529 E−11	3.88
640×640	1.9116 E−6	1.94	5.5156 E−12	3.72
1280×1280	4.8873 E−7	1.97	2.3093 E−12	1.26
Grid	$E_{\nabla y}$: DPM2	Rate	$E_{\nabla y}$: DPM4	Rate
80×80	5.0079 E−5	—	1.7467 E−8	—
160×160	1.2601 E−5	1.99	7.8108 E−10	4.48
320×320	2.9763 E−6	2.08	3.6291 E−11	4.43
640×640	7.5893 E−7	1.97	2.7711 E−12	3.71
1280×1280	1.7966 E−7	2.08	9.2371 E−13	1.58

TABLE 6.3. *Grid convergence in the approximate solution and components of the discrete gradient for BDF2-DPM2 and BDF4-DPM4. The interior domain is the circle with $R=1$ centered at the origin and the exterior domain is $\Omega_1=[-2,2]\times[-2,2]\backslash\Omega_2$. Test problem (6.5), (6.9) with material coefficients $\lambda_1=\lambda_2=1$. The dimension of the set of basis functions is $\mathcal{N}_1^0+\mathcal{N}_1^1=15$.*

Grid	E: DPM2	Rate	E: DPM4	Rate
80×80	7.6881 E−4	—	3.6981 E−6	—
160×160	1.3587 E−4	2.50	1.3966 E−7	4.73
320×320	3.0556 E−5	2.15	6.9116 E−9	4.34
640×640	7.0384 E−6	2.12	4.7680 E−10	3.86
1280×1280	1.4834 E−6	2.25	2.9068 E−11	4.04
Grid	$E_{\nabla x}$: DPM2	Rate	$E_{\nabla x}$: DPM4	Rate
80×80	3.5415 E−3	—	1.8532 E−5	—
160×160	8.4177 E−4	2.07	1.1510 E−6	4.01
320×320	2.5576 E−4	1.72	5.9865 E−8	4.27
640×640	9.1801 E−5	1.48	4.1454 E−9	3.85
1280×1280	2.4652 E−5	1.90	3.0029 E−10	3.79
Grid	$E_{\nabla y}$: DPM2	Rate	$E_{\nabla y}$: DPM4	Rate
80×80	1.1226 E−3	—	1.4928 E−5	—
160×160	4.4288 E−4	1.34	8.7078 E−7	4.10
320×320	1.1094 E−4	2.00	2.9190 E−8	4.90
640×640	2.9997 E−5	1.89	1.6709 E−9	4.13
1280×1280	8.1752 E−6	1.88	1.0353 E−10	4.01

TABLE 6.4. *Grid convergence in the approximate solution and components of the discrete gradient for BDF2-DPM2 and BDF4-DPM4. The interior domain Ω_2 is the ellipse with $a=1$, $b=0.5$ centered at the origin, and the exterior domain is $\Omega_1=[-2,2]\times[-2,2]\backslash\Omega_2$. Test problem (6.5), (6.9) with material coefficients $\lambda_1=\lambda_2=1$. The dimension of the set of basis functions is $\mathcal{N}_1^0+\mathcal{N}_1^1=14$.*

Grid	E: DPM2	Rate	E: DPM4	Rate
80×80	7.6881 E−4	—	3.6981 E−6	—
160×160	1.3563 E−4	2.50	1.3966 E−7	4.73
320×320	3.0555 E−5	2.15	6.9115 E−9	4.34
640×640	7.0382 E−6	2.12	4.7555 E−10	3.86
1280×1280	1.4823 E−6	2.25	2.6223 E−11	4.18
Grid	$E_{\nabla x}$: DPM2	Rate	$E_{\nabla x}$: DPM4	Rate
80×80	6.2981 E−3	—	2.7304 E−5	—
160×160	1.2811 E−3	2.30	1.6395 E−6	4.06
320×320	3.4898 E−4	1.88	7.1143 E−8	4.53
640×640	1.1413 E−4	1.61	6.4634 E−9	3.46
1280×1280	2.8904 E−5	1.98	4.4645 E−10	3.86
Grid	$E_{\nabla y}$: DPM2	Rate	$E_{\nabla y}$: DPM4	Rate
80×80	1.3998 E−3	—	1.5733 E−5	—
160×160	4.4540 E−4	1.65	9.3488 E−7	4.07
320×320	1.1094 E−4	2.01	3.4802 E−8	4.75
640×640	2.9998 E−5	1.89	2.0272 E−9	4.10
1280×1280	8.1753 E−6	1.88	1.3403 E−10	3.92

TABLE 6.5. *Grid Convergence in the approximate solution and components of the discrete gradient for BDF2-DPM2 and BDF4-DPM4. The interior domain Ω_2 is the ellipse with $a=1,b=0.5$ centered at the origin, and the exterior domain is $\Omega_1=[-2,2]\times[-2,2]\backslash\Omega_2$. Test problem (6.5), (6.9) with material coefficients $\lambda_1=\lambda_2=1$ and mixed boundary conditions at the boundary $\partial\Omega_1$ (Dirichlet boundary condition on $x=\pm2$ and Neumann boundary condition on $y=\pm2$). The dimension of the set of basis functions is $\mathcal{N}_1^0+\mathcal{N}_1^1=14$.*

Grid	E: DPM2	Rate	E: DPM4	Rate
80×80	7.9812 E−4	—	2.9898 E−6	—
160×160	1.4009 E−4	2.51	2.0200 E−7	3.89
320×320	3.1875 E−5	2.14	1.1593 E−8	4.12
640×640	7.3395 E−6	2.12	7.1578 E−10	4.02
1280×1280	1.5469 E−6	2.25	4.2984 E−11	4.06
Grid	$E_{\nabla x}$: DPM2	Rate	$E_{\nabla x}$: DPM4	Rate
80×80	3.7071 E−3	—	1.1915 E−5	—
160×160	8.7074 E−4	2.09	1.1238 E−6	3.41
320×320	2.7019 E−4	1.69	8.1536 E−8	3.78
640×640	9.7094 E−5	1.48	6.4286 E−9	3.66
1280×1280	2.6201 E−5	1.89	4.5029 E−10	3.84
Grid	$E_{\nabla y}$: DPM2	Rate	$E_{\nabla y}$: DPM4	Rate
80×80	1.1155 E−3	—	1.4438 E−5	—
160×160	4.4213 E−4	1.34	8.0955 E−7	4.16
320×320	1.1064 E−4	2.00	2.9929 E−8	4.76
640×640	2.9948 E−5	1.89	1.8004 E−9	4.06
1280×1280	8.1714 E−6	1.87	1.0894 E−10	4.05

TABLE 6.6. *Grid convergence in the approximate solution and components of the discrete gradient for BDF2-DPM2 and BDF4-DPM4. The interior domain Ω_2 is the ellipse with $a=1$, $b=0.5$ centered at the origin, and the exterior domain is $\Omega_1=[-2,2]\times[-2,2]\backslash\Omega_2$. Test problem (6.5), (6.9) with material coefficients $\lambda_1=1000,\lambda_2=1$. The dimension of the set of basis functions is $\mathcal{N}_1^0+\mathcal{N}_1^1=14$.*

Grid	E: DPM2	Rate	E: DPM4	Rate
80×80	1.4217 E−3	—	7.4403 E−6	—
160×160	2.9665 E−4	2.26	4.0478 E−7	4.20
320×320	7.3169 E−5	2.02	1.9894 E−8	4.35
640×640	1.7889 E−5	2.03	1.2509 E−9	3.99
1280×1280	4.1268 E−6	2.12	7.5583 E−11	4.05
Grid	$E_{\nabla x}$: DPM2	Rate	$E_{\nabla x}$: DPM2	Rate
80×80	3.8663 E−3	—	1.9899 E−5	—
160×160	1.0083 E−3	1.94	1.4353 E−6	3.79
320×320	2.8264 E−4	1.83	7.2317 E−8	4.31
640×640	8.7710 E−5	1.69	4.8302 E−9	3.90
1280×1280	2.2856 E−5	1.94	3.2323 E−10	3.90
Grid	$E_{\nabla y}$: DPM2	Rate	$E_{\nabla y}$: DPM2	Rate
80×80	1.4592 E−3	—	1.5954 E−5	—
160×160	5.4385 E−4	1.42	1.0272 E−6	3.96
320×320	1.3660 E−4	1.99	3.9502 E−8	4.70
640×640	3.5267 E−5	1.95	2.4817 E−9	3.99
1280×1280	9.3338 E−6	1.92	1.6533 E−10	3.91

TABLE 6.7. *Grid convergence in the approximate solution and components of the discrete gradient for BDF2-DPM2 and BDF4-DPM4. The interior domain Ω_2 is the ellipse with $a=1$, $b=0.5$ centered at the origin, and the exterior domain is $\Omega_1=[-2,2]\times[-2,2]\backslash\Omega_2$. Test problem (6.5), (6.9) with material coefficients $\lambda_1=1,\lambda_2=1000$. The dimension of the set of basis functions is $\mathcal{N}_1^0+\mathcal{N}_1^1=14$.*

Grid	E: DPM2	Rate	$E_{\nabla x}$: DPM2	Rate	$E_{\nabla y}$: DPM2	Rate
80×80	7.4073 E−4	—	3.4746 E−3	—	1.1400 E−3	—
160×160	1.2603 E−4	2.56	8.3667 E−4	2.05	4.4737 E−4	1.35
320×320	2.8324 E−5	2.15	2.4533 E−4	1.77	1.0918 E−4	2.03
640×640	6.5472 E−6	2.11	9.0596 E−5	1.44	2.9761 E−5	1.88
1280×1280	1.3770 E−6	2.25	2.4439 E−5	1.89	8.1312 E−6	1.87

TABLE 6.8. *Grid convergence in the approximate solution and components of the discrete gradient for TR-DPM2. The interior domain Ω_2 is the ellipse with $a=1$, $b=0.5$ centered at the origin, and the exterior domain is $\Omega_1=[-2,2]\times[-2,2]\backslash\Omega_2$. Test problem (6.5), (6.9) with material coefficients $\lambda_1=\lambda_2=1$. The dimension of the set of basis functions is $\mathcal{N}_1^0+\mathcal{N}_1^1=14$.*

The interior and exterior domains for all the tests below are selected as:

$$\Omega_2=\frac{x^2}{a^2}+\frac{y^2}{b^2}<1,$$
$$\Omega_1=[-1,1]\times[-1,1]\setminus\Omega_2 \text{ in Tables 6.1-6.2 and,}$$
$$\Omega_1=[-2,2]\times[-2,2]\setminus\Omega_2 \text{ in Tables 6.3-6.19.}$$

Hence, the interface between the two subdomains Ω_1 and Ω_2 is defined as:

$$\Gamma:\quad \frac{x^2}{a^2}+\frac{y^2}{b^2}=1 \tag{6.6}$$

Also, in the tests in Tables 6.1-6.2 we employ for DPM2 and DPM4 the following auxiliary domains:

$$\Omega_2^0=[-1,1]\times[-1,1],$$
$$\Omega_1^0=[-1,1]\times[-1,1], \text{ and}$$

Grid	E: DPM2	Rate	E: DPM4	Rate
80×80	1.0135 E−3	—	7.4246 E−6	—
160×160	3.5331 E−4	1.52	6.6548 E−7	3.48
320×320	6.6191 E−5	2.42	1.1037 E−7	2.59
640×640	1.5269 E−5	2.12	4.0942 E−9	4.75
1280×1280	3.3138 E−6	2.20	2.3671 E−10	4.11
Grid	$E_{\nabla x}$: DPM2	Rate	$E_{\nabla x}$: DPM4	Rate
80×80	5.9560 E−3	—	5.6133 E−5	—
160×160	3.0166 E−3	0.98	7.4232 E−6	2.92
320×320	8.0478 E−4	1.91	1.9217 E−6	1.95
640×640	2.9206 E−4	1.46	5.6177 E−8	5.10
1280×1280	8.3292 E−5	1.81	4.2715 E−9	3.72
Grid	$E_{\nabla y}$: DPM2	Rate	$E_{\nabla y}$: DPM4	Rate
80×80	8.8393 E−4	—	1.0822 E−5	—
160×160	1.8939 E−3	−1.10	6.4538 E−6	0.75
320×320	4.1076 E−4	2.20	1.6162 E−6	2.00
640×640	1.0743 E−4	1.93	3.9642 E−8	5.35
1280×1280	2.9308 E−5	1.87	2.0309 E−9	4.29

TABLE 6.9. *Grid convergence in the approximate solution and components of the discrete gradient for BDF2-DPM2 and BDF4-DPM4. The interior domain Ω_2 is the ellipse with $a=1$, $b=0.25$ centered at the origin, and the exterior domain is $\Omega_1=[-2,2]\times[-2,2]\backslash\Omega_2$. Test problem (6.5), (6.9) with material coefficients $\lambda_1=\lambda_2=1$. The dimension of the set of basis functions is $\mathcal{N}_1^0+\mathcal{N}_1^1=14$.*

Grid	E: DPM2	Rate	E: DPM4	Rate
80×80	1.1025 E−1	—	4.8459 E−2	—
160×160	2.6875 E−2	2.04	1.4713 E−3	5.04
320×320	6.8304 E−3	1.98	8.0078 E−5	4.20
640×640	1.6937 E−3	2.01	4.3420 E−6	4.20
1280×1280	4.2290 E−4	2.00	2.6202 E−7	4.05
Grid	$E_{\nabla x}$: DPM2	Rate	$E_{\nabla x}$: DPM4	Rate
80×80	1.0007	—	2.1336 E−1	—
160×160	2.5093 E−1	2.00	1.3739 E−2	3.96
320×320	6.4225 E−2	1.97	7.5298 E−4	4.19
640×640	1.5953 E−2	2.01	4.0899 E−5	4.20
1280×1280	3.9995 E−3	2.00	2.5927 E−6	3.98
Grid	$E_{\nabla y}$: DPM2	Rate	$E_{\nabla y}$: DPM4	Rate
80×80	1.6609	—	4.1642 E−1	—
160×160	4.7529 E−1	1.81	2.1383 E−2	4.28
320×320	1.2658 E−1	1.91	1.3405 E−3	4.00
640×640	3.1638 E−2	2.00	8.1454 E−5	4.04
1280×1280	7.8696 E−3	2.01	4.8436 E−6	4.07

TABLE 6.10. *Grid convergence in the approximate solution and components of the discrete gradient for BDF2-DPM2 and BDF4-DPM4. The interior domain is the circle with $R=1$ centered at the origin and the exterior domain is $\Omega_1=[-2,2]\times[-2,2]\backslash\Omega_2$. Test problem (6.5), (6.10) with material coefficients $\lambda_1=\lambda_2=1$. The dimension of the set of basis functions is $\mathcal{N}_2^0+\mathcal{N}_2^1=2$.*

in all the tests in Tables 6.3–6.19 we employ for DPM2 and DPM4 the following auxiliary domains:

$$\Omega_2^0=[-2,2]\times[-2,2],$$
$$\Omega_1^0=[-2,2]\times[-2,2].$$

Grid	E: DPM2	Rate	E: DPM4	Rate
80×80	1.1021 E−1	—	4.8460 E−2	—
160×160	2.6941 E−2	2.03	1.4713 E−3	5.04
320×320	6.8303 E−3	1.98	8.0078 E−5	4.20
640×640	1.7103 E−3	2.00	4.4226 E−6	4.18
1280×1280	4.3016 E−4	1.99	2.7469 E−7	4.01
Grid	$E_{\nabla x}$: DPM2	Rate	$E_{\nabla x}$: DPM4	Rate
80×80	1.0007	—	2.1335 E−1	—
160×160	2.5093 E−1	2.00	1.3739 E−2	3.96
320×320	6.4225 E−2	1.97	7.5298 E−4	4.19
640×640	1.5953 E−2	2.01	4.0899 E−5	4.20
1280×1280	3.9851 E−3	2.00	2.4691 E−6	4.05
Grid	$E_{\nabla y}$: DPM2	Rate	$E_{\nabla y}$: DPM4	Rate
80×80	1.6609	—	4.1640 E−1	—
160×160	4.7403 E−1	1.81	2.1383 E−2	4.28
320×320	1.2658 E−1	1.90	1.3405 E−3	4.00
640×640	3.5818 E−2	1.82	8.1454 E−5	4.04
1280×1280	8.9701 E−3	2.00	4.8436 E−6	4.07

TABLE 6.11. *Grid convergence in the approximate solution and components of the discrete gradient for BDF2-DPM2 and BDF4-DPM4. The interior domain Ω_2 is the ellipse with $a=1$, $b=0.5$ centered at the origin, and the exterior domain is $\Omega_1=[-2,2]\times[-2,2]\backslash\Omega_2$. Test problem (6.5), (6.10) with material coefficients $\lambda_1=\lambda_2=1$. The dimension of the set of basis functions is $\mathcal{N}_2^0+\mathcal{N}_2^1=3$.*

Grid I	Grid II	E: DPM2	Rate	E: DPM4	Rate
160×160	40×40	2.7142 E−2	—	1.4713 E−3	—
320×320	80×80	6.8358 E−3	1.99	8.0078 E−5	4.20
640×640	160×160	1.7250 E−3	1.99	4.4570 E−6	4.17
1280×1280	320×320	4.3347 E−4	1.99	2.7579 E−7	4.01
Grid I	Grid II	$E_{\nabla x}$: DPM2	Rate	$E_{\nabla x}$: DPM4	Rate
160×160	40×40	2.5093 E−1	—	1.3739 E−2	—
320×320	80×80	6.4225 E−2	1.97	7.5298 E−4	4.19
640×640	160×160	1.5953 E−2	2.01	4.0899 E−5	4.20
1280×1280	320×320	3.9851 E−3	2.00	2.4691 E−6	4.05
Grid I	Grid II	$E_{\nabla y}$: DPM2	Rate	$E_{\nabla y}$: DPM4	Rate
160×160	40×40	4.7450 E−1	—	2.1383 E−2	—
320×320	80×80	1.2658 E−1	1.91	1.3405 E−3	4.00
640×640	160×160	3.6066 E−2	1.81	8.1454 E−5	4.04
1280×1280	320×320	9.0284 E−3	2.00	4.8436 E−6	4.07

TABLE 6.12. *Grid convergence in the approximate solution and components of the discrete gradient for BDF2-DPM2 and BDF4-DPM4. The interior domain Ω_2 is the ellipse with $a=1$, $b=0.5$ centered at the origin, and the exterior domain is $\Omega_1=[-2,2]\times[-2,2]\backslash\Omega_2$. Test problem (6.5), (6.10) with material coefficients $\lambda_1=\lambda_2=1$. The dimension of the set of basis functions is $\mathcal{N}_2^0+\mathcal{N}_2^1=3$. Non-matching meshes for Ω_1 (Grid I) and Ω_2 (Grid II).*

We consider time interval $[0,T]$ with $T=0.1$ as the final time. The time step was set as $\Delta t=0.5h$ for the methods.

For the test in Table 6.1, the exact solution is defined as (see Figure 6.1, left plot):

$$u(x,y,t)=\begin{cases} u_1(x,y,t)=e^t\left(\left(16x^2/\pi^2+36y^2/\pi^2\right)^{5/2}/10-1/10+1\right), & (x,y)\in\Omega_1,\\ u_2(x,y,t)=e^t\left(16x^2/\pi^2+36y^2/\pi^2\right)^{5/2}, & (x,y)\in\Omega_2. \end{cases} \tag{6.7}$$

Grid	E: DPM2	Rate	E: DPM4	Rate
80×80	1.1247 E−1	—	4.5922 E−2	—
160×160	2.7736 E−2	2.02	1.4668 E−3	4.97
320×320	7.2126 E−3	1.94	9.7493 E−5	3.91
640×640	1.8600 E−3	1.96	6.1556 E−6	3.99
1280×1280	4.6821 E−4	1.99	3.8729 E−7	3.99
Grid	$E_{\nabla x}$: DPM2	Rate	$E_{\nabla x}$: DPM4	Rate
80×80	1.0142	—	1.9462 E−1	—
160×160	2.5334 E−1	2.00	1.3300 E−2	3.87
320×320	6.5334 E−2	1.96	7.3914 E−4	4.17
640×640	1.6360 E−2	2.00	4.2018 E−5	4.14
1280×1280	4.1011 E−3	2.00	2.5568 E−6	4.04
Grid	$E_{\nabla y}$: DPM2	Rate	$E_{\nabla y}$: DPM4	Rate
80×80	1.6682	—	3.9898 E−1	—
160×160	4.7259 E−1	1.82	1.9675 E−2	4.34
320×320	1.2611 E−1	1.91	1.2806 E−3	3.94
640×640	3.7275 E−2	1.76	7.9745 E−5	4.01
1280×1280	9.4443 E−3	1.98	5.0201 E−6	3.99

TABLE 6.13. *Grid convergence in the approximate solution and components of the discrete gradient for BDF2-DPM2 and BDF4-DPM4. The interior domain Ω_2 is the ellipse with $a=1$, $b=0.5$ centered at the origin, and the exterior domain is $\Omega_1=[-2,2]\times[-2,2]\backslash\Omega_2$. Test problem (6.5), (6.10) with material coefficients $\lambda_1=1000,\lambda_2=1$. The dimension of the set of basis functions is $\mathcal{N}_2^0+\mathcal{N}_2^1=3$.*

Grid	E: DPM2	Rate	E: DPM4	Rate
80×80	1.1021 E−1	—	4.8460 E−2	—
160×160	2.6938 E−2	2.03	1.4713 E−3	5.04
320×320	6.8303 E−3	1.98	8.0078 E−5	4.20
640×640	1.7116 E−3	2.00	4.4229 E−6	4.18
1280×1280	4.3106 E−4	1.99	2.7473 E−7	4.01
Grid	$E_{\nabla x}$: DPM2	Rate	$E_{\nabla x}$: DPM4	Rate
80×80	1.0007	—	2.1335 E−1	—
160×160	2.5093 E−1	2.00	1.3739 E−2	3.96
320×320	6.4225 E−2	1.97	7.5298 E−4	4.19
640×640	1.5953 E−2	2.01	4.0899 E−5	4.20
1280×1280	3.9851 E−3	2.00	2.4691 E−6	4.05
Grid	$E_{\nabla y}$: DPM2	Rate	$E_{\nabla y}$: DPM4	Rate
80×80	1.6609	—	4.1640 E−1	—
160×160	4.7402 E−1	1.81	2.1383 E−2	4.28
320×320	1.2658 E−1	1.90	1.3405 E−3	4.00
640×640	3.5813 E−2	1.82	8.1454 E−5	4.04
1280×1280	8.9737 E−3	2.00	4.8436 E−6	4.07

TABLE 6.14. *Grid convergence in the approximate solution and components of the discrete gradient for BDF2-DPM2 and BDF4-DPM4. The interior domain Ω_2 is the ellipse with $a=1$, $b=0.5$ centered at the origin, and the exterior domain is $\Omega_1=[-2,2]\times[-2,2]\backslash\Omega_2$. Test problem (6.5), (6.10) with material coefficients $\lambda_1=1,\lambda_2=1000$. The dimension of the set of basis functions is $\mathcal{N}_2^0+\mathcal{N}_2^1=3$.*

For the test in Table 6.2, the exact solution is defined (see Figure 6.1, right plot)

$$u(x,y,t)=\begin{cases} u_1(x,y,t)=e^t\left(16x^2/\pi^2+36y^2/\pi^2\right)^{5/2}, & (x,y)\in\Omega_1,\\ \\ u_2(x,y,t)=e^t\left(16x^2/\pi^2+36y^2/\pi^2\right)^{5/2}. & (x,y)\in\Omega_2. \end{cases} \tag{6.8}$$

Grid	E: DPM2	Rate	E: DPM4	Rate
80×80	1.1021 E−1	—	4.8460 E−2	—
160×160	2.6873 E−2	2.04	1.4713 E−3	5.04
320×320	6.8303 E−3	1.98	8.0078 E−5	4.20
640×640	1.6937 E−3	2.01	4.3420 E−6	4.20
1280×1280	4.2290 E−4	2.00	2.6887 E−7	4.01
Grid	$E_{\nabla x}$: DPM2	Rate	$E_{\nabla x}$: DPM4	Rate
80×80	1.0007	—	2.1335 E−1	—
160×160	2.5093 E−1	2.00	1.3739 E−2	3.96
320×320	6.4225 E−2	1.97	7.5298 E−4	4.19
640×640	1.5953 E−2	2.01	4.0899 E−5	4.20
1280×1280	3.9851 E−3	2.00	2.4691 E−6	4.05
Grid	$E_{\nabla y}$: DPM2	Rate	$E_{\nabla y}$: DPM4	Rate
80×80	1.6754	—	4.1640 E−1	—
160×160	4.7478 E−1	1.82	2.1383 E−2	4.28
320×320	1.2658 E−1	1.91	1.3405 E−3	4.00
640×640	3.4376 E−2	1.88	8.1454 E−5	4.04
1280×1280	9.3278 E−3	1.88	4.8436 E−6	4.07

TABLE 6.15. *Grid convergence in the approximate solution and components of the discrete gradient for BDF2-DPM2 and BDF4-DPM4. The interior domain Ω_2 is the ellipse with $a=1$, $b=0.25$ centered at the origin, and the exterior domain is $\Omega_1=[-2,2]\times[-2,2]\backslash\Omega_2$. Test problem (6.5), (6.10) with material coefficients $\lambda_1=\lambda_2=1$. The dimension of the set of basis functions is $\mathcal{N}_2^0+\mathcal{N}_2^1=3$.*

The exact solution (6.7) for the problem (6.5) with $\lambda_1=10$ and $\lambda_2=1$ is continuous across the interface $\Gamma: x^2/(\pi^2/16)+y^2/(\pi^2/36)=1$, and also has continuous flux across the interface (the exact solution (6.7) is a modified version of the solution for the parabolic interface problem from [26]). The exact solution (6.8) for the problem (6.5) with $\lambda_1=10$ and $\lambda_2=1$ is continuous across the interface Γ, but has the discontinuous flux across the interface. The reader can consult [21, 22] for the analytical results for the parabolic interface problems under continuity assumption on the solution at the interface boundary. As one can see from Tables 6.1–6.2, DPM2 and DPM4 reconstruct solutions and gradient of the solutions to (6.5)-(6.7) and to (6.5)-(6.8) with the second-order and fourth-order accuracy, respectively.

For the next several tests in Tables 6.3–6.9, the exact solution is defined as (see Figure 6.2):

$$u(x,y,t)=\begin{cases} u_1(x,y,t)=e^{-t}\sin x\cos y, & (x,y)\in\Omega_1,\\ u_2(x,y,t)=e^{-t}(x^2-y^2), & (x,y)\in\Omega_2. \end{cases} \tag{6.9}$$

(the exact solution (6.9) is a modified version of the exact solution for the elliptic interface problem from [25]). Next, the exact solution for the test problem in Tables 6.10–6.15 below is similar to the exact solution (6.9) but has a much higher frequency (oscillations) in the exterior subdomain Ω_1, and is defined as (see also Figure 6.2):

$$u(x,y,t)=\begin{cases} u_1(x,y,t)=e^{-t}\sin(3\pi x)\cos(7\pi y), & (x,y)\in\Omega_1,\\ u_2(x,y,t)=e^{-t}(x^2-y^2), & (x,y)\in\Omega_2. \end{cases} \tag{6.10}$$

Next, in Tables 6.16–6.17, we consider additional tests with the exact solution

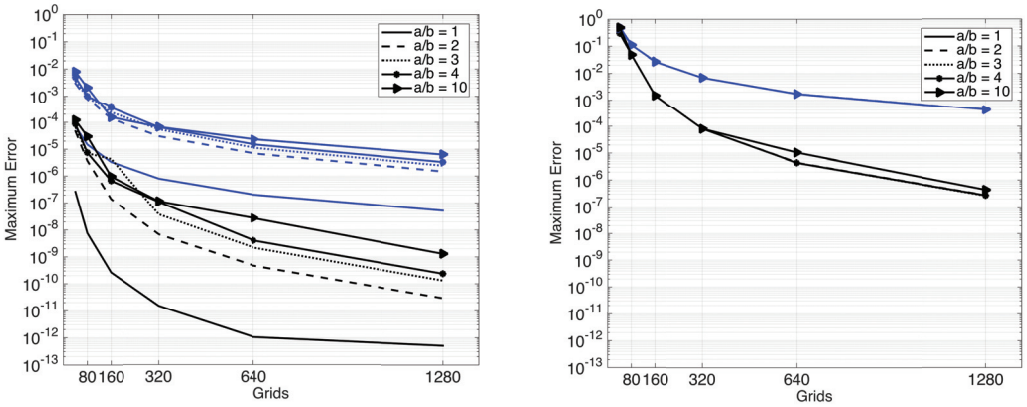

FIG. 6.4. *Grid convergence using BDF2-DPM2 (blue) and BDF4-DPM4 (black) is compared for several different interfaces* $\Gamma: x^2/a^2 + y^2/b^2 = 1$ *with increasing aspect ratios* a/b. *The results are presented for the test problem (6.5), (6.9) with material coefficients* $\lambda_1 = \lambda_2 = 1$ *(left figure) and for the test problem (6.5), (6.10) with material coefficients* $\lambda_1 = \lambda_2 = 1$ *(right figure). Similar results are produced by DPM for the same test problems but with different material coefficients in different subdomains, as well as for error in the gradient of the solution.*

Grid	E: DPM2	Rate	E: DPM4	Rate
160×160	1.9789 E−4	—	2.7787 E−7	—
320×320	4.7654 E−5	2.05	1.6946 E−8	4.04
640×640	1.2033 E−5	1.99	1.0478 E−9	4.02
1280×1280	3.0447 E−6	1.98	6.6320 E−11	3.98
Grid	$E_{\nabla x}$: DPM2	Rate	$E_{\nabla x}$: DPM4	Rate
160×160	4.0263 E−4	—	8.3030 E−7	—
320×320	9.8635 E−5	2.03	5.1278 E−8	4.02
640×640	2.4795 E−5	1.99	3.2037 E−9	4.00
1280×1280	6.2404 E−6	1.99	2.0147 E−10	3.99
Grid	$E_{\nabla y}$: DPM2	Rate	$E_{\nabla y}$: DPM4	Rate
160×160	4.5444 E−4	—	7.8078 E−7	—
320×320	1.0952 E−4	2.05	4.9491 E−8	3.98
640×640	2.7244 E−5	2.01	3.1439 E−9	3.98
1280×1280	6.9267 E−6	1.98	1.9934 E−10	3.98

TABLE 6.16. *Grid convergence in the approximate solution and components of the discrete gradient for BDF2-DPM2 and BDF4-DPM4. The interior domain* Ω_2 *is the ellipse with* $a = 1$, $b = 0.5$ *centered at the origin, and the exterior domain is* $\Omega_1 = [-2,2] \times [-2,2] \backslash \Omega_2$. *Test problem (6.5), (6.11) with material coefficients* $\lambda_1 = \lambda_2 = 1$. *The dimension of the set of basis functions is* $\mathcal{N}_1^0 + \mathcal{N}_1^1 = 30$.

defined as (see also Figure 6.3):

$$u(x,y,t) = \begin{cases} u_1(x,y,t) = \frac{1}{1+t^2}\,\frac{1}{1+x^2+y^2}, & (x,y) \in \Omega_1, \\ \\ u_2(x,y,t) = \frac{2}{1+t^2}\,\frac{1}{1+x^2+y^2}, & (x,y) \in \Omega_2. \end{cases} \tag{6.11}$$

Finally, the exact solution $u(x,y,t)$ for the test problem in Tables 6.18–6.19 has jump conditions at the interface that oscillate in time and $u(x,y,t)$ is described below (see

Grid	E: DPM2	Rate	E: DPM4	Rate
160×160	2.8136 E−4	—	3.5928 E−7	—
320×320	7.0314 E−5	2.00	2.3179 E−8	3.95
640×640	1.7684 E−5	1.99	1.4809 E−9	3.97
1280×1280	4.4399 E−6	1.99	9.5923 E−11	3.95
Grid	$E_{\nabla x}$: DPM2	Rate	$E_{\nabla x}$: DPM4	Rate
160×160	4.7849 E−4	—	8.8373 E−7	—
320×320	1.2038 E−4	1.99	5.5880 E−8	3.98
640×640	3.0157 E−5	2.00	3.5157 E−9	3.99
1280×1280	7.5442 E−6	2.00	2.2297 E−10	3.98
Grid	$E_{\nabla y}$: DPM2	Rate	$E_{\nabla y}$: DPM4	Rate
160×160	6.0641 E−4	—	9.4720 E−7	—
320×320	1.5331 E−4	1.98	5.9268 E−8	4.00
640×640	4.0266 E−5	1.93	3.7796 E−9	3.97
1280×1280	1.0680 E−5	1.91	2.4475 E−10	3.95

TABLE 6.17. *Grid convergence in the approximate solution and components of the discrete gradient for BDF2-DPM2 and BDF4-DPM4. The interior domain Ω_2 is the ellipse with $a=1$, $b=0.5$ centered at the origin, and the exterior domain is $\Omega_1=[-2,2]\times[-2,2]\backslash\Omega_2$. Test problem (6.5), (6.11) with material coefficients $\lambda_1=1,\lambda_2=1000$ (example of the different material coefficients). The dimension of the set of basis functions is $\mathcal{N}_1^0+\mathcal{N}_1^1=30$.*

Grid	E: DPM2	Rate	E: DPM4	Rate
160×160	9.9762 E−3	—	6.7679 E−4	—
320×320	1.8988 E−3	2.39	3.3825 E−5	4.32
640×640	3.5081 E−4	2.44	1.7882 E−6	4.24
1280×1280	8.3125 E−5	2.08	1.0675 E−7	4.07
Grid	$E_{\nabla x}$: DPM2	Rate	$E_{\nabla x}$: DPM4	Rate
160×160	3.8474 E−2	—	2.6405 E−3	—
320×320	9.2627 E−3	2.05	1.9427 E−4	3.76
640×640	3.0389 E−3	1.61	1.3134 E−5	3.89
1280×1280	8.4412 E−4	1.85	8.9533 E−7	3.87
Grid	$E_{\nabla y}$: DPM2	Rate	$E_{\nabla y}$: DPM4	Rate
160×160	4.8148 E−2	—	2.8102 E−3	—
320×320	1.8412 E−2	1.39	2.6349 E−4	3.41
640×640	4.9064 E−3	1.91	2.1896 E−5	3.59
1280×1280	1.3661 E−3	1.84	1.6539 E−6	3.73

TABLE 6.18. *Grid convergence in the approximate solution and components of the discrete gradient for BDF2-DPM2 and BDF4-DPM4. The interior domain Ω_2 is the ellipse with $a=1$, $b=0.5$ centered at the origin, and the exterior domain is $\Omega_1=[-2,2]\times[-2,2]\backslash\Omega_2$. Test problem (6.5), (6.12) with material coefficients $\lambda_1=\lambda_2=1$. The dimension of the set of basis functions is $\mathcal{N}_1^0+\mathcal{N}_1^1=2$.*

also Figure 6.3):

$$u(x,y,t)=\begin{cases} u_1(x,y,t)=0, \ \ (x,y)\in\Omega_1, \\ \\ u_2(x,y,t)=1000\sin(10\pi t)x^4y^5, \ \ (x,y)\in\Omega_2. \end{cases} \tag{6.12}$$

In the tests in Tables 6.1–6.7 and Tables 6.9–6.19 we consider BDF2 as the time discretization for DPM2, and BDF4 as the time discretization for DPM4. Similar to [3], we also tested the proposed high-order methods in space using the trapezoidal scheme (TR) as the time discretization. We obtained very similar results between BDF2-DPM2

Grid	E: DPM2	Rate	E: DPM4	Rate
160×160	1.2679 E−2	—	1.7861 E−4	—
320×320	3.2972 E−3	1.94	1.1429 E−5	3.97
640×640	7.5776 E−4	2.12	7.0576 E−7	4.02
1280×1280	1.7516 E−4	2.11	4.2724 E−8	4.05
Grid	$E_{\nabla x}$: DPM2	Rate	$E_{\nabla x}$: DPM4	Rate
160×160	4.6315 E−2	—	3.2243 E−4	—
320×320	1.3103 E−2	1.82	2.1652 E−5	3.90
640×640	3.3175 E−3	1.98	1.4078 E−6	3.94
1280×1280	7.9967 E−4	2.05	9.4477 E−8	3.90
Grid	$E_{\nabla y}$: DPM2	Rate	$E_{\nabla y}$: DPM4	Rate
160×160	8.3000 E−2	—	6.0763 E−4	—
320×320	2.7938 E−2	1.57	4.0041 E−5	3.92
640×640	6.8421 E−3	2.03	2.5456 E−6	3.98
1280×1280	1.6947 E−3	2.01	1.5769 E−7	4.01

TABLE 6.19. *Grid convergence in the approximate solution and components of the discrete gradient for BDF2-DPM2 and BDF4-DPM4. The interior domain Ω_2 is the ellipse with $a=1$, $b=0.5$ centered at the origin, and the exterior domain is $\Omega_1=[-2,2]\times[-2,2]\backslash\Omega_2$. Test problem (6.5), (6.12) with material coefficients $\lambda_1=1,\lambda_2=1000$ (example of the different material coefficients). The dimension of the set of basis functions is $\mathcal{N}_1^0+\mathcal{N}_1^1=2$.*

and TR-DPM2, as well as between BDF4-DPM4 and TR-DPM4. To illustrate this with an example, we give Table 6.8 for TR-DPM2 that can be compared with results in Table 6.4 for BDF2-DPM2 on the same test problem. Note that similarly, the accuracy of BDF4-DPM4 and TR-DPM4 was in very close agreement on all the tests we considered. However, TR-DPM4 is much more computationally expensive since it is only second-order accurate in time, and the required time step $\Delta t=O(h^2)$ is much smaller than the time step $\Delta t=O(h)$ needed for BDF4-DPM4 to maintain fourth-order accuracy in space.

In all the numerical experiments presented in Tables 6.3–6.19, we consider curves Γ (6.6) with different aspect ratios a/b as the interface between subdomains. Note, that we also performed the same tests using a circle ($a=b$) as the interface curve, and obtained a similar convergence rate: second-order and fourth-order convergence rate in the maximum error in the solution, as well as in the maximum error in the discrete gradient of the solution for DPM2 and DPM4, respectively. In Table 6.3, the slow down in the convergence rate for DPM4 on finer meshes is due to the loss of significant digits, as the absolute level of error gets close to machine zero, and in Table 6.9, the mesh has to be fine enough to obtain the expected convergence rates due to already relatively high aspect ratio of the interface curve ($\Gamma: x^2+16y^2=1$) for the test problem in the table. Furthermore, the results presented in Figure 6.4 show that the convergence rate in DPM (DPM2 and DPM4) on parabolic interface models is not affected by the size of the aspect ratio of the considered circular/elliptical domains (we obtained overall second- and fourth-order accuracy on the tests considered). Moreover, the accuracy of DPM2 and DPM4 is not affected by the size of the jump ratio in the diffusion coefficients as can be seen from the Tables 6.4–6.7, Tables 6.11, 6.13–6.14 and Tables 6.16–6.19 or by the considered boundary conditions, see Tables 6.4-6.5. Moreover, as shown in Tables 6.11–6.12, the method is well-suited for domain decomposition approaches or adaptive simulations. In particular, in Tables 6.11–6.12, we show that when we use a much coarser mesh in the domain Ω_2 with the less oscillatory solution, we obtain an accuracy

which is very close to the accuracy we achieved while using the same fine mesh in both domains. All these features demonstrate great robustness and high-order accuracy of the designed numerical schemes for the interface problems (similar properties of DPM2 and DPM4 were shown for the elliptic interface problems [2, 11, 12, 40]).

Results in Tables 6.1–6.19 for DPM2 and DPM4 illustrate overall second-order and fourth-order rate of convergence, respectively, in the maximum error in the solution and in the maximum error in the discrete gradient of the solution to the parabolic interface problems. *This high-order accuracy of DPM2, and in particular of DPM4, and the efficiency of numerical algorithms based on Difference Potentials are crucial for time-dependent problems where lower-order methods can fail to resolve delicate features of the solutions to model problems [3, 4, 13].*

7. Conclusion

In this paper, we developed efficient high-order accurate methods in time and space based on Difference Potentials for 2D parabolic interface/composite domain models. We gave the construction of high-order accurate methods based on Difference Potentials for single domain, and for the interface/composite domain problems with non-matching interface conditions. The constructed numerical algorithms are not restricted by the choice of boundary or interface conditions, and the main computational complexity of the designed algorithms reduces to the several solutions of simple auxiliary problems on regular structured grids. The methods can handle with ease non-matching grids for the subdomains/domains and are well-suited for parallel computations. Moreover, similar to [2,3,12], 2D numerical tests clearly confirm the capability of the Difference Potentials approach to resolve discontinuities with high-order accuracy at the material interfaces.

At this point the developed methods are constructed for problems in 2D domains with smooth fixed curvilinear interfaces represented by closed curves. For near future and future research, we plan to develop h-adaptive algorithms based on the Difference Potentials approach and extend methods to models that have possible geometric singularities at the interface boundaries as well as to moving/evolving boundary/interface problems. We also plan to extend developed methods to nonlinear models in 2D and 3D.

Appendix.

A.1. Details of the time discretization.. For the reader's convenience we present below details of the time-discrete scheme (3.7). The coefficient σ^2 below is the same as on the left-handside of (3.7):

(1) Trapezoidal scheme in time:
In case of the trapezoidal scheme in time, the linear operator $L_{\Delta t}[u^{i+1}]$ is defined in (3.8), and the right-hand side F^{i+1} in (3.7) takes the form:

$$F^{i+1} := -\frac{1}{\lambda}\Big(f(x,y,t^{i+1}) + f(x,y,t^{i})\Big) - \Big(\Delta + \sigma^2 \mathbb{I}\Big)u^{i}. \tag{7.1}$$

(2) The second-order backward difference scheme (BDF2) in time:
In case of the second-order backward difference scheme (BDF2) in time, the linear operator $L_{\Delta t}[u^{i+1}]$ is defined in (3.8) (similarly to the Trapezoidal scheme in time), and the right-hand side F^{i+1} in (3.7) for BDF2 takes the form:

$$F^{i+1} := -\frac{1}{\lambda} f(x,y,t^{i+1}) - \frac{\sigma^2}{3}(4u^{i} - u^{i-1}). \tag{7.2}$$

(3) The fourth-order backward difference scheme (BDF4) in time:
In case of the fourth-order backward difference scheme (BDF4) in time, the linear operator $L_{\Delta t}[u^{i+1}]$ is defined in (3.8) (similarly to the Trapezoidal and BDF2 schemes in time), and the right-hand side F^{i+1} in (3.7) for BDF4 takes the form:

$$F^{i+1} := -\frac{1}{\lambda} f(x,y,t^{i+1}) - \frac{\sigma^2}{25}(48u^i - 36u^{i-1} + 16u^{i-2} - 3u^{i-3}). \tag{7.3}$$

A.2. Details of the construction of the extension operators.. Here, we give details of the construction of the extension operators (3.25) and (3.26) for the case of the circular and elliptical domains. The idea of the construction is based on the knowledge of the continuous PDE model (3.1) and the use of Cauchy data u_Γ^{i+1} at time t^{i+1}. Very similar construction extends to domains with general curvilinear boundaries (the difference will be in the choice of the parametrization/local coordinates).

(1) *Example of the construction of the extension operator in the case of circular domains, and polar coordinates* (r,θ) *as the parametrization of* Γ*:* The parabolic equation in (3.1) can be rewritten in standard polar coordinates (r,θ) as:

$$\frac{\partial u}{\partial t} - \lambda\left(\frac{\partial^2 u}{\partial r^2} + \frac{1}{r}\frac{\partial u}{\partial r} + \frac{1}{r^2}\frac{\partial^2 u}{\partial \theta^2}\right) = f. \tag{7.4}$$

The coordinate r corresponds to the distance from the origin along the normal direction $\mathbf{n}$ to the circular interface Γ. Hence, extension operators (3.25)–(3.26) are equivalent to:

$$\pi_{\gamma\Gamma}[\mathrm{u}_\Gamma^{i+1}]|_{(x_j,y_k)} \equiv u_{j,k}^{i+1}(r_0,\theta) = u\Big|_\Gamma + d\frac{\partial u}{\partial r}\Big|_\Gamma + \frac{d^2}{2}\frac{\partial^2 u}{\partial r^2}\Big|_\Gamma, \quad (x_j,y_k)\in\gamma \tag{7.5}$$

and

$$\begin{aligned}\pi_{\gamma\Gamma}[\mathrm{u}_\Gamma^{i+1}]|_{(x_j,y_k)} \equiv u_{j,k}^{i+1}(r_0,\theta) = u\Big|_\Gamma + d\frac{\partial u}{\partial r}\Big|_\Gamma + \frac{d^2}{2!}\frac{\partial^2 u}{\partial r^2}\Big|_\Gamma + \frac{d^3}{3!}\frac{\partial^3 u}{\partial r^3}\Big|_\Gamma \\ + \frac{d^4}{4!}\frac{\partial^4 u}{\partial r^4}\Big|_\Gamma, \quad (x_j,y_k)\in\gamma,\end{aligned} \tag{7.6}$$

where, as before, $d = r - r_0$ denotes the *signed* distance from a grid point $(x_j,y_k)\in\gamma$ on the radius r, to the nearest point $(x,y)\in\Gamma$ on the original circle corresponding to the radius r_0. The higher-order derivatives $\frac{\partial^e u}{\partial r^e}$, $e = 2,3,...$ on Γ at time t^{i+1} in (7.5)–(7.6) can be obtained through the Cauchy data $(u(\theta,t^{i+1})|_\Gamma, \frac{\partial u}{\partial r}(\theta,t^{i+1})|_\Gamma)$, and the consecutive differentiation of the governing differential Equation (7.4) with respect to r as illustrated below:

$$\frac{\partial^2 u}{\partial r^2} = \frac{1}{\lambda}\Big(\frac{\partial u}{\partial t} - f\Big) - \frac{1}{r^2}\frac{\partial^2 u}{\partial \theta^2} - \frac{1}{r}\frac{\partial u}{\partial r}. \tag{7.7}$$

The expression (7.7) for $\frac{\partial^2 u}{\partial r^2}$ is used in the 3–term extension operator (7.5) in the second-order method, and is used in the 5–term extension operator (7.6) in the fourth-order method.

Similarly, in the 5–term extension operator (7.6), terms $\frac{\partial^3 u}{\partial r^3}$ and $\frac{\partial^4 u}{\partial r^4}$ are replaced by the following expressions:

$$\frac{\partial^3 u}{\partial r^3} = \frac{1}{\lambda}\left(\frac{\partial^2 u}{\partial r \partial t} - \frac{\partial f}{\partial r}\right) + \frac{2}{r^2}\frac{\partial u}{\partial r} - \frac{1}{r^2}\frac{\partial^3 u}{\partial r \partial \theta^2} - \frac{1}{r\lambda}\left(\frac{\partial u}{\partial t} - f\right) + \frac{3}{r^3}\frac{\partial^2 u}{\partial \theta^2} \tag{7.8}$$

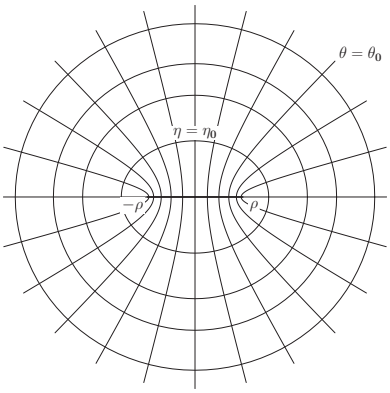

FIG. 7.1. *Sketch of the elliptical coordinate system: distance from the center of the ellipse to either foci - ρ; isoline - η; elliptical angle - θ, [2].*

$$\begin{aligned}\frac{\partial^4 u}{\partial r^4} =& \frac{1}{\lambda}\left(\frac{\partial^3 u}{\partial r^2 \partial t} - \frac{\partial^2 f}{\partial r^2}\right) - \frac{4}{r^3}\frac{\partial u}{\partial r} + \frac{2}{r^2}\frac{\partial^2 u}{\partial r^2} + \frac{1}{r^2\lambda}\left(\frac{\partial u}{\partial t} - f\right) \\ & - \frac{1}{r\lambda}\left(\frac{\partial^2 u}{\partial r \partial t} - \frac{\partial f}{\partial r}\right) - \frac{9}{r^4}\frac{\partial^2 u}{\partial \theta^2} + \frac{5}{r^3}\frac{\partial^3 u}{\partial r \partial \theta^2} - \frac{1}{r^2}\frac{\partial^4 u}{\partial r^2 \partial \theta^2}\end{aligned} \tag{7.9}$$

where $\frac{\partial^4 u}{\partial r^2 \partial \theta^2}$ is given by

$$\frac{\partial^4 u}{\partial r^2 \partial \theta^2} = \frac{1}{\lambda}\left(\frac{\partial^3 u}{\partial \theta^2 \partial t} - \frac{\partial^2 f}{\partial \theta^2}\right) - \frac{1}{r}\frac{\partial^3 u}{\partial r \partial \theta^2} + \frac{1}{r^2}\frac{\partial^4 u}{\partial \theta^4}. \tag{7.10}$$

(2) *Example of the construction of the extension operator in the case of elliptical domains, and elliptical coordinates (η,θ) as the parametrization of Γ:* Analogously to the above case of a circular domain, for the case of the domain where boundary Γ is defined by an ellipse $x^2/a^2 + y^2/b^2 = 1$, one possible convenient choice is to employ elliptical coordinates as the parametrization, and represent the extension operators (3.25)–(3.26) using such parametrization (see also [2, 31]).

Recall, that an elliptical coordinate system with coordinates (η,θ) is given by the standard transformation:

$$x = \rho \cosh\eta \cos\theta \tag{7.11}$$

$$y = \rho \sinh\eta \sin\theta \tag{7.12}$$

where $\eta \geq 0$ and $0 \leq \theta < 2\pi$, see Figure 7.1. Also, recall that the distance from the center of the ellipse to either foci is defined as $\rho = \sqrt{a^2 - b^2}$.
In elliptical coordinates, the constant $\eta = \eta_0 \equiv \frac{1}{2}\ln\frac{a+b}{a-b}$, the coordinate line (isoline), is given by the ellipse:

$$\frac{x^2}{\rho^2 \cosh^2\eta_0} + \frac{y^2}{\rho^2 \sinh^2\eta_0} = 1.$$

Similarly, for constant $\theta = \theta_0$, the coordinate line is defined by the hyperbola:

$$\frac{x^2}{\rho^2 \cos^2\theta_0} - \frac{y^2}{\rho^2 \sin^2\theta_0} = \cosh^2\eta - \sinh^2\eta = 1.$$

Now, let us recall that for the choice of elliptical coordinates the basis vectors are defined as:

$$\hat{\eta} = (\rho \sinh\eta \cos\theta, \rho \cosh\eta \sin\theta) \tag{7.13}$$

$$\hat{\theta} = (-\rho \cosh\eta \sin\theta, \rho \sinh\eta \cos\theta). \tag{7.14}$$

The corresponding Lame coefficients in both directions are equivalent to $H = \rho\sqrt{\sinh^2\eta + \sin^2\theta}$. Consequently, the elliptic operator in (3.1) can be rewritten in the standard elliptical coordinates (η,θ) as:

$$\Delta_{\eta,\theta} = \frac{1}{H^2}\left(\frac{\partial^2}{\partial\eta^2} + \frac{\partial^2}{\partial\theta^2}\right). \tag{7.15}$$

Hence, the parabolic Equation (3.1) in elliptical coordinates become:

$$\frac{\partial u}{\partial t} - \frac{\lambda}{H^2}\left(\frac{\partial^2 u}{\partial\eta^2} + \frac{\partial^2 u}{\partial\theta^2}\right) = f. \tag{7.16}$$

Similarly to the above example of a circular domain, the smooth extension operators (3.25)–(3.26) are equivalent to:

$$\pi_{\gamma\Gamma}[\mathrm{u}_\Gamma^{i+1}]|_{(x_j,y_k)} \equiv u_{j,k}^{i+1}(\eta_0,\theta) = u\Big|_\Gamma + d\frac{\partial u}{\partial\eta}\Big|_\Gamma + \frac{d^2}{2}\frac{\partial^2 u}{\partial\eta^2}\Big|_\Gamma, \quad (x_j,y_k)\in\gamma \tag{7.17}$$

and

$$\begin{aligned}\pi_{\gamma\Gamma}[\mathrm{u}_\Gamma^{i+1}]|_{(x_j,y_k)} \equiv u_{j,k}^{i+1}(\eta_0,\theta) = u\Big|_\Gamma + d\frac{\partial u}{\partial\eta}\Big|_\Gamma + \frac{d^2}{2!}\frac{\partial^2 u}{\partial\eta^2}\Big|_\Gamma + \frac{d^3}{3!}\frac{\partial^3 u}{\partial\eta^3}\Big|_\Gamma \\ + \frac{d^4}{4!}\frac{\partial^4 u}{\partial\eta^4}\Big|_\Gamma, \quad (x_j,y_k)\in\gamma\end{aligned} \tag{7.18}$$

where, again as before, $d = \eta - \eta_0$ denotes the *signed* distance from a grid point $(x_j,y_k)\in\gamma$ on the coordinate line η, to the nearest point $(x,y)\in\Gamma$ on the original ellipse corresponding to the contour line η_0.

At time t^{i+1}, the higher-order derivatives $\frac{\partial^e u}{\partial\eta^e}$, $e = 2,3,...$ on Γ in (7.17)–(7.18) can be obtained through the Cauchy data $(u(\theta,t^{i+1})|_\Gamma, \frac{\partial u}{\partial\eta}(\theta,t^{i+1})|_\Gamma)$, and the consecutive differentiation of the governing differential Equation (7.16) with respect to η as illustrated below (note that in polar coordinates we had that $\frac{\partial u}{\partial n} = \frac{\partial u}{\partial r}$, but in elliptical coordinates we have $\frac{\partial u}{\partial n} = \frac{1}{H}\frac{\partial u}{\partial\eta}$):

$$\frac{\partial^2 u}{\partial\eta^2} = \frac{H^2}{\lambda}\left(\frac{\partial u}{\partial t} - f\right) - \frac{\partial^2 u}{\partial\theta^2}. \tag{7.19}$$

The higher order terms, $\frac{\partial^3 u}{\partial\eta^3}$ and $\frac{\partial^4 u}{\partial\eta^4}$ are obtained by consecutive differentiation of (7.19).

$$\frac{\partial^3 u}{\partial\eta^3} = 2\frac{H}{\lambda}\frac{\partial H}{\partial\eta}\left(\frac{\partial u}{\partial t} - f\right) + \frac{H^2}{\lambda}\left(\frac{\partial^2 u}{\partial\eta\partial t} - \frac{\partial f}{\partial\eta}\right) - \frac{\partial^3 u}{\partial\eta\partial\theta^2} \tag{7.20}$$

$$\frac{\partial^4 u}{\partial\eta^4} = \frac{2}{\lambda}\left(\left(\frac{\partial H}{\partial\eta}\right)^2 + H\frac{\partial^2 H}{\partial\eta^2}\right)\left(\frac{\partial u}{\partial t} - f\right) + 4\frac{H}{\lambda}\frac{\partial H}{\partial\eta}\left(\frac{\partial^2 u}{\partial\eta\partial t} - \frac{\partial f}{\partial\eta}\right)$$

$$+\frac{H^2}{\lambda}\left(\frac{\partial^3 u}{\partial\eta^2\partial t}-\frac{\partial^2 f}{\partial\eta^2}\right)-\frac{\partial^4 u}{\partial\eta^2\partial\theta^2} \tag{7.21}$$

where $\frac{\partial^4 u}{\partial\eta^2\partial\theta^2}$ is given by:

$$\begin{aligned}\frac{\partial^4 u}{\partial\eta^2\partial\theta^2}=&\frac{2}{\lambda}\left(\left(\frac{\partial H}{\partial\theta}\right)^2+H\frac{\partial^2 H}{\partial\theta^2}\right)\left(\frac{\partial u}{\partial t}-f\right)+\frac{4}{\lambda}H\frac{\partial H}{\partial\theta}\left(\frac{\partial^2 u}{\partial\theta\partial t}-\frac{\partial f}{\partial\theta}\right)\\&+\frac{H^2}{\lambda}\left(\frac{\partial^3 u}{\partial\theta^2\partial t}-\frac{\partial^2 f}{\partial\theta^2}\right)-\frac{\partial^4 u}{\partial\theta^4}.\end{aligned} \tag{7.22}$$

Note, that in formula (7.21) terms that include second-order partial derivation with respect to η are replaced by the expressions given in (7.19) and in (7.22).

To approximate the time derivatives and mixed time-space derivatives appearing in (7.7)–(7.9) and (7.19)–(7.21) in terms of the Cauchy data, we use the following backward-in-time finite difference approximations (note that terms $\frac{\partial^3 u}{\partial r^2\partial t}$ in (7.9) and $\frac{\partial^3 u}{\partial\eta^2\partial t}$ in (7.21) are determined in our algorithm by differentiating in time (7.7) and (7.19) respectively, but finite-differences can be employed too). The formulas (7.23)–(7.24) are employed if we consider second-order discretization in time for (3.1)–(3.3):

$$\frac{\partial u}{\partial t}(x_j,y_k,t^{i+1})\approx\frac{3u_{j,k}^{i+1}-4u_{j,k}^{i}+u_{j,k}^{i-1}}{2\Delta t} \tag{7.23}$$

$$\frac{\partial^2 u}{\partial t^2}(x_j,y_k,t^{i+1})\approx\frac{2u_{j,k}^{i+1}-5u_{j,k}^{i}+4u_{j,k}^{i-1}-u_{j,k}^{i-2}}{(\Delta t)^2}. \tag{7.24}$$

In the case of the fourth-order discretization in time for (3.1)–(3.3), we use the corresponding higher-order backward difference formulas:

$$\frac{\partial u}{\partial t}(x_j,y_k,t^{i+1})\approx\frac{25u_{j,k}^{i+1}-48u_{j,k}^{i}+36u_{j,k}^{i-1}-16u_{j,k}^{i-2}+3u_{j,k}^{i-3}}{12\Delta t} \tag{7.25}$$

$$\begin{aligned}\frac{\partial^2 u}{\partial t^2}(x_j,y_k,t^{i+1})\approx&\frac{1}{\Delta t^2}\left(\frac{15}{4}u_{j,k}^{i+1}-\frac{77}{6}u_{j,k}^{i}+\frac{107}{6}u_{j,k}^{i-1}\right.\\&\left.-13u_{j,k}^{i-2}+\frac{61}{12}u_{j,k}^{i-3}-\frac{5}{6}u_{j,k}^{i-3}\right).\end{aligned} \tag{7.26}$$

Acknowledgements. The authors are grateful to the anonymous referees for the careful reading of the paper and for their most valuable comments, suggestions and questions that helped to improve the manuscript.

The research of Jason Albright, Yekaterina Epshteyn and Qing Xia was supported in part by the National Science Foundation Grant # DMS-1112984. The research of Yekaterina Epshteyn is also supported in part by Simons Foundation Award #415673. The research of Jason Albright was also supported in part through the University of Utah Graduate Research Fellowship.

REFERENCES

[1] Loyce Adams and Zhilin Li, *The immersed interface/multigrid methods for interface problems*, SIAM J. Sci. Comput., 24(2):463–479 (electronic), 2002.

[2] J. Albright, Y. Epshteyn, M. Medvinsky, and Q. Xia, *High-order numerical schemes based on difference potentials for 2d elliptic problems with material interfaces*, Appl. Numer. Math., 111:64-91, 2015.

[3] J. Albright, Y. Epshteyn, and K.R. Steffen, *High-order accurate difference potentials methods for parabolic problems*, Appl. Numer. Math., 93:87–106, 2015.

[4] Jason Albright, *Numerical methods based on difference potentials for models with material interfaces*, Ph.D. Dissertation, in progress.

[5] Ivo Babuška, *The finite element method for elliptic equations with discontinuous coefficients*, Computing (Arch. Elektron. Rechnen), 5:207–213, 1970.

[6] D.S. Britt, S.V. Tsynkov, and E. Turkel, *A high-order numerical method for the Helmholtz equation with nonstandard boundary conditions*, SIAM J. Sci. Comput., 35(5):A2255–A2292, 2013.

[7] Zhiming Chen and Jun Zou, *Finite element methods and their convergence for elliptic and parabolic interface problems*, Numer. Math., 79(2):175–202, 1998.

[8] Armando Coco and Giovanni Russo, *Second order multigrid methods for elliptic problems with discontinuous coefficients on an arbitrary interface, I: One dimensional problems*, Numer. Math. Theory Methods Appl., 5(1):19–42, 2012.

[9] R.K. Crockett, P. Colella, and D.T. Graves, *A Cartesian grid embedded boundary method for solving the Poisson and heat equations with discontinuous coefficients in three dimensions*, J. Comput. Phys., 230(7):2451–2469, 2011.

[10] Y. Epshteyn, *Upwind-difference potentials method for Patlak–Keller–Segel chemotaxis model*, Journal of Scientific Computing, 53(3):689–713, 2012.

[11] Y. Epshteyn and M. Medvinsky, *On the solution of the elliptic interface problems by difference potentials method*, Lecture Notes in Computational Science and Engineering, Springer Series, 106:197–205, 2015.

[12] Y. Epshteyn and S. Phippen, *High-order difference potentials methods for 1D elliptic type models*, Appl. Numer. Math., 93:69–86, July 2015.

[13] Yekaterina Epshteyn, *Algorithms composition approach based on difference potentials method for parabolic problems*, Commun. Math. Sci., 12(4):723–755, 2014.

[14] Yekaterina Epshteyn, Ivan Sofronov, and Semyon Tsynkov, *Professor V. S. Ryaben'kii. On the occasion of the 90-th birthday [Editorial]*, Appl. Numer. Math., 93:1–2, 2015.

[15] Frédéric Gibou and Ronald Fedkiw, *A fourth order accurate discretization for the Laplace and heat equations on arbitrary domains, with applications to the Stefan problem*, J. Comput. Phys., 202(2):577–601, 2005.

[16] S.K. Godunov, V.T. Zhukov, M.I. Lazarev, I.L. Sofronov, V.I. Turchaninov, A.S. Kholodov, S.V. Tsynkov, B.N. Chetverushkin, and Y.Y. Epshteyn, *Viktor Solomonovich Ryaben'kii and his School*, Uspekhi Mat. Nauk (Russian Math. Surveys), 70:213–236, 2015.

[17] Arthur Guittet, Mathieu Lepilliez, Sebastien Tanguy, and Frédéric Gibou, *Solving elliptic problems with discontinuities on irregular domains—the Voronoi interface method*, J. Comput. Phys., 298:747–765, 2015.

[18] Jeffrey Lee Hellrung, Jr., Luming Wang, Eftychios Sifakis, and Joseph M. Teran, *A second order virtual node method for elliptic problems with interfaces and irregular domains in three dimensions*, J. Comput. Phys., 231(4):2015–2048, 2012.

[19] D.S. Kamenetskiĭ and V.S. Ryaben′kiĭ, *Solution of boundary value problems for the Laplace equation in a domain with a cut by the method of difference potentials*, Akad. Nauk SSSR Inst. Prikl. Mat. preprint, (33):24, 1990.

[20] Juri D. Kandilarov and Lubin G. Vulkov, *The immersed interface method for two-dimensional heat-diffusion equations with singular own sources*, Appl. Numer. Math., 57(5-7):486–497, 2007.

[21] O.A. Ladyženskaja, V. Ja. Rivkind, and N.N. Ural′ceva, *Classical solvability of diffraction problems for equations of elliptic and parabolic types*, Dokl. Akad. Nauk SSSR, 158:513–515, 1964.

[22] O.A. Ladyženskaja, V. Ja. Rivkind, and N.N. Ural′ceva, *Solvability of diffraction problems in the classical sense*, Trudy Mat. Inst. Steklov., 92:116–146, 1966.

[23] Randall J. LeVeque and Zhi Lin Li, *The immersed interface method for elliptic equations with discontinuous coefficients and singular sources*, SIAM J. Numer. Anal., 31(4):1019–1044, 1994.

[24] Randall J. LeVeque and Zhilin Li, *Immersed interface methods for Stokes flow with elastic boundaries or surface tension*, SIAM J. Sci. Comput., 18(3):709–735, 1997.

[25] Zhilin Li and Kazufumi Ito, *The Immersed Interface Method*, Frontiers in Applied Mathematics, 33, Society for Industrial and Applied Mathematics (SIAM), Philadelphia, PA, 2006.

[26] Tao Lin, Qing Yang, and Xu Zhang, *Partially penalized immersed finite element methods for parabolic interface problems*, Numerical Methods for Partial Differential Equations,

31(6):1925–1947, 2015.

[27] Xu-Dong Liu, Ronald P. Fedkiw, and Myungjoo Kang, *A boundary condition capturing method for Poisson's equation on irregular domains*, J. Comput. Phys., 160(1):151–178, 2000.

[28] Xu-Dong Liu and Thomas C. Sideris, *Convergence of the ghost fluid method for elliptic equations with interfaces*, Math. Comp., 72(244):1731–1746 (electronic), 2003.

[29] J. Loncaric, V.S. Ryaben'kii, and S.V. Tsynkov, *Active shielding and control of noise*, SIAM J. Appl. Math., 62(2):563–596 (electronic), 2001.

[30] Anita Mayo, *The fast solution of Poisson's and the biharmonic equations on irregular regions*, SIAM J. Numer. Anal., 21(2):285–299, 1984.

[31] M. Medvinsky, S. Tsynkov, and E. Turkel, *The method of difference potentials for the Helmholtz equation using compact high order schemes*, J. Sci. Comput., 53(1):150–193, 2012.

[32] Emmanuel A. Ntumy and Sergey V. Utyuzhnikov, *Active sound control in composite regions*, Appl. Numer. Math., 234(1):215-C223, 2014.

[33] Charles S. Peskin, *Numerical analysis of blood flow in the heart*, J. Comput. Phys., 25(3):220–252, 1977.

[34] Charles S. Peskin, *The immersed boundary method*, Acta Numer., 11:479–517, 2002.

[35] A.A. Reznik, *Approximation of surface potentials of elliptic operators by difference potentials*, Dokl. Akad. Nauk SSSR, 263(6):1318–1321, 1982.

[36] A.A. Reznik, *Approximation of surface potentials of elliptic operators by difference potentials and solution of boundary value problems*, Ph.D, Moscow, MPTI, 1983.

[37] V.S. Ryaben′kiĭ, *Boundary equations with projections*, Uspekhi Mat. Nauk, 40(2(242)):121–149, 238, 1985.

[38] V.S. Ryaben′kiĭ, *Difference potentials analogous to Cauchy integrals*, Uspekhi Mat. Nauk, 67(3(405)):147–172, 2012.

[39] V.S. Ryaben'kii and S.V. Tsynkov, *Artificial boundary conditions for the numerical solution of external viscous flow problems*, SIAM J. Numer. Anal., 32(5):1355–1389, 1995.

[40] V.S. Ryaben′kiĭ, V.I. Turchaninov, and E. Yu. Èpshteĭn, *An algorithm composition scheme for problems in composite domains based on the method of difference potentials*, Zh. Vychisl. Mat. Mat. Fiz., (10):1853–1870, 2006.

[41] V.S. Ryaben′kii. *Method of difference potentials and its applications*, Springer Series in Computational Mathematics, Springer-Verlag, Berlin, 30, 2002.

[42] V.S. Ryaben'kii, V.I. Turchaninov, and Ye. Yu. Epshteyn, *The numerical example of algorithms composition for solution of the boundary-value problems on compound domain based on difference potential method*, Moscow, Keldysh Institute for Applied Mathematics, Russia Academy of Sciences, (3), 2003.

[43] Rajen Kumar Sinha and Bhupen Deka, *Optimal error estimates for linear parabolic problems with discontinuous coefficients*, SIAM J. Numer. Anal., 43(2):733–749 (electronic), 2005.

[44] S. Tsynkov, *Numerical solution of problems on unbounded domains. A review*, Appl. Numer. Math., 27(4):465–532, 1998. Absorbing boundary conditions.

[45] Eddie Wadbro, Sara Zahedi, Gunilla Kreiss, and Martin Berggren, *A uniformly well-conditioned, unfitted Nitsche method for interface problems*, BIT, 53(3):791–820, 2013.

[46] Sining Yu, Yongcheng Zhou, and G.W. Wei, *Matched interface and boundary (MIB) method for elliptic problems with sharp-edged interfaces*, J. Comput. Phys., 224(2):729–756, 2007.

[47] S. Zahedi, E. Wadbro, G. Kreiss, and M. Berggren, *A uniformly well-conditioned, unfitted nitsche method for interface problems: Part I*, subbmited, 2013.

[48] Y.C. Zhou, Shan Zhao, Michael Feig, and G.W. Wei, *High order matched interface and boundary method for elliptic equations with discontinuous coefficients and singular sources*, J. Comput. Phys., 213(1):1–30, 2006.